Realia et naturalia

DISSERTATIONES
PHYSICAE
UNIVERSITATIS
TARTUENSIS
87

PEETER PIKSARV

Spatiotemporal characterization of diffractive and non-diffractive light pulses

TARTU ÜLIKOOL · UNIVERSITAS TARTUENSIS · 1632

DISSERTATIONES PHYSICAE UNIVERSITATIS TARTUENSIS
87

DISSERTATIONES PHYSICAE UNIVERSITATIS TARTUENSIS
87

PEETER PIKSARV

Spatiotemporal characterization of diffractive and non-diffractive light pulses

UNIVERSITY OF TARTU
PRESS
1632

The study was carried out at the Institute of Physics, University of Tartu, Estonia.

The dissertation was admitted on May 31, 2013, in partial fulfilment of the requirements for the degree of Doctor of Philosophy in Physics, and was allowed for defence by the Council of the Institute of Physics, University of Tartu.

Supervisor: Prof. Acad. Peeter Saari
Institute of Physics, University of Tartu
Tartu, Estonia

Opponents: Prof. Kishan Dholakia
School of Physics and Astronomy, University of St. Andrews
St. Andrews, Scotland, United Kingdom

Dr. Cord L. Arnold
Division of Atomic Physics, Lund University
Lund, Sweden

Defence: September 6, 2013, University of Tartu, Estonia

Publication of this thesis was financially supported by the graduate school "Functional materials and technologies" receiving funding from the European Social Fund under project 1.2.0401.09-0079 in Estonia.

ISSN 1406–0647
ISBN 978–9949–32–325–8 (print)
ISBN 978–9949–32–326–5 (pdf)

University of Tartu Press
www.tyk.ee
Order No. 253

CONTENTS

List of original publications **7**

1. Introduction **11**

2. Diffractive and non-diffractive light pulses **15**
2.1. Bessel-type waves 15
2.1.1. Bessel-X pulses 16
2.1.2. Accelerating Bessel pulses 17
2.1.3. Pulsed Bessel beam 17
2.2. Boundary diffraction wave 19
2.2.1. Boundary diffraction wave for plane wave pulses . . . 20
2.2.2. Boundary diffraction wave for Gaussian pulses 23
2.3. Airy pulses 24

3. Spectral interferometric ultrashort pulse characterization techniques **27**
3.1. Spectral interferometry 28
3.2. Spatial spectral interferometry 29
3.3. SEA TADPOLE 32

4. Results and discussion **35**
4.1. Bessel-X pulses [I, IV, V] 36
4.2. Accelerating Bessel pulses [II, IV] 38
4.3. Pulsed Bessel beam [VIII, IX] 39
4.4. Boundary diffraction wave [III–VII] 42
4.5. Airy pulses [X] 45

Summary **49**

Summary in Estonian **51**

Acknowledgements **53**

References **55**

Publications **65**

Curriculum vitae **151**

LIST OF ORIGINAL PUBLICATIONS

This thesis is based on the following papers, which are referred to in the text by their Roman numerals.

I P. Bowlan, H. Valtna-Lukner, M. Lõhmus, **P. Piksarv**, P. Saari, and R. Trebino, "Measuring the spatiotemporal field of ultrashort Bessel-X pulses," Opt. Lett. **34**, 2276–2278 (2009).

II H. Valtna-Lukner, P. Bowlan, M. Lõhmus, **P. Piksarv**, R. Trebino, and P. Saari, "Direct spatiotemporal measurements of accelerating ultrashort Bessel-type light bullets," Opt. Express **17**, 14948–14955 (2009).

III M. Lõhmus, P. Bowlan, R. Trebino, H. Valtna-Lukner, **P. Piksarv**, and P. Saari, "Directly recording diffraction phenomena in the time domain," Lith. J. Phys **50**, 69–74 (2010).

IV P. Saari, P. Bowlan, H. Valtna-Lukner, M. Lõhmus, **P. Piksarv**, and R. Trebino, "Time-and-space-domain study of diffracting and non-diffracting light pulses," Lith. J. Phys **50**, 121–127 (2010).

V P. Saari, P. Bowlan, H. Valtna-Lukner, M. Lõhmus, **P. Piksarv**, and R. Trebino, "Directly recording diffraction phenomena in time domain," Laser Phys. **20**, 948–953 (2010).

VI P. Saari, P. Bowlan, H. Valtna-Lukner, M. Lõhmus, **P. Piksarv**, and R. Trebino, "Basic diffraction phenomena in time domain," Opt. Express **18**, 11083–11088 (2010).

VII **P. Piksarv**, P. Bowlan, M. Lõhmus, H. Valtna-Lukner, R. Trebino, and P. Saari, "Diffraction of ultrashort Gaussian pulses within the framework of boundary diffraction wave theory," J. Opt. **14**, 015701 (2012).

VIII M. Lõhmus, P. Bowlan, **P. Piksarv**, H. Valtna-Lukner, R. Trebino, and P. Saari, "Diffraction of ultrashort optical pulses from circularly symmetric binary phase gratings," Opt. Lett. **37**, 1238–1240 (2012).

IX **P. Piksarv**, H. Valtna-Lukner, A. Valdmann, M. Lõhmus, R. Matt, and P. Saari, "Temporal focusing of ultrashort pulsed Bessel beams into Airy–Bessel light bullets," Opt. Express **20**, 17220–17229 (2012).

X **P. Piksarv**, A. Valdmann, H. Valtna-Lukner, R. Matt, and P. Saari, "Spatiotemporal characterization of ultrabroadband Airy pulses," Opt. Lett. **38**, 1143–1145 (2013).

List of other publications

This list contains other relevant publications, that are not included as a part of this thesis.

XI P. Bowlan, R. Trebino, H. Valtna-Lukner, M. Lõhmus, **P. Piksarv**, and P. Saari, "Directly measuring the spatiotemporal electric field of ultrashort Bessel-X pulses," in *Conference on Lasers and Electro-Optics/International Quantum Electronics Conference (CLEO/QELS)*, (Optical Society of America, 2009), paper CThW6.

XII **P. Piksarv**, P. Bowlan, M. Lõhmus, H. Valtna-Lukner, R. Trebino, and P. Saari, "Propagation of ultrashort pulses behind diffracting screens," in *22nd Congress of ICO: Light for the Development of the World*, R. Rodríguez-Vera and R. Díaz-Uribe, eds., Proc. SPIE **8011**, 801130 (2011).

XIII **P. Piksarv**, H. Valtna-Lukner, A. Valdmann, M. Lõhmus, R. Matt, and P. Saari, "Measuring the temporal focusing of ultrashort Airy–Bessel wave packets," in *25th IEEE Photonics Conference (IPC)*, (IEEE, 2012), pp. 497–498.

XIV **P. Piksarv**, H. Valtna-Lukner, A. Valdmann, M. Lõhmus, R. Matt, and P. Saari, "Measuring the suppresion of ultrashort pulses into Airy–Bessel light bullets with almost single-cycle temporal resolution," in *XVIIIth International Conference on Ultrafast Phenomena*, M. Chergui, A. Taylor, S. Cundiff, R. de Vivie-Riedle, and K. Yamanouchi, eds., EPJ Web of Conferences **41**, 10022 (2013).

XV P. Bowlan, H. Valtna-Lukner, M. Lõhmus, **P. Piksarv**, P. Saari, and R. Trebino, "Measurement of the spatiotemporal electric field of ultrashort superluminal Bessel-X pulses," Opt. Photon. News **20**, 42 (2009).

Author's contribution

The papers on which this thesis is based are the result of collective work and contain important contributions from all the co-authors. The author's contribution to the publications referred to by their Roman numerals is indicated as follows:

I Consulting during the measurements, numerical simulations, and data analysis.

II Participating in carrying out the experiments. Consulting during the numerical simulations and data analysis. Preparing Figs. 2 and 3 of the manuscript.

III Participating in carrying out the experiments, the numerical simulations, and data analysis.

IV Participating in carrying out the experiments. Consulting during the numerical simulations and data analysis. Preparing Fig. 2 of the manuscript.

V Participating in carrying out the experiments, the numerical simulations, and data analysis. Preparing Figs. 2, 3 and 5 of the manuscript.

VI Participating in carrying out the experiments, the numerical simulations, and data analysis. Preparing Figs. 2, 3, 4, and the multimedia files of the manuscript. Writing a part of the manuscript.

VII The lead author of the publication. Participating in carrying out the experiments, theoretical derivation, the numerical simulations, and data analysis. Writing the manuscript and preparing the figures.

VIII Participating in carrying out the experiments. Consulting during the numerical simulations and data analysis.

IX The lead author of the publication. Participating in carrying out the experiments, developing the measurement method, the numerical simulations, and data analysis. Writing the manuscript and preparing the figures.

X The lead author of the publication. Participating in carrying out the experiments, the numerical simulations, and data analysis. Writing the manuscript and preparing the figures and multimedia files.

1. INTRODUCTION

Ultrashort laser pulses have become an invaluable tool in many areas of science and technology; they are one of the shortest events ever created by humankind. Lasers that produce pulses shorter than 6 fs ($1\,\mathrm{fs} = 10^{-15}\,\mathrm{s}$) in duration and lasting only a few optical cycles have become commercially available. The spectrum of such ultrafast events spans over an octave in the visible region. Furthermore, for numerous applications, high spatial localization of pulses is desired, in addition to temporal localization. Both diffractive and dispersive broadening of laser pulses are inevitable and make achieving such spatiotemporal localization of broadband pulses more than a challenging task. However, a certain set of solutions exists to the wave equation that have a tight maximum which propagates seemingly unaffected by the diffraction and/or dispersion. These wave packets are called non-diffractive or localized waves, see, e.g. collective monographs [1, 2].

In addition to the prolonged depth of focus, the localized waves have many useful properties that may seem intriguing or somewhat controversial. These include superluminal propagation or even acceleration of the pulse maximum in free space and self-reconstruction behind obstacles. The monochromatic non-diffracting Bessel beams—the basic building blocks for the non-diffractive waves—have been widely studied and applied since the pioneering work by Durnin in 1987 [3, 4]. Similarly, after the first experimental evidence of superluminally propagating Bessel-X pulses a decade later [5], the subject of non-diffractive pulsed waves has evolved into a mature field with emerging applications. For example, the non-spreading peak of non-diffracting localized high-power laser pulses has proven necessary to record weak Hawking radiation from an optical analogue of an astrophysical black hole evaporation [6, 7]. In addition, Bessel pulses have become useful tools in imaging [8], micromachining [9, 10], and cell transfection [11]. Even the newest addition to the non-diffractive family—the seemingly curvilinearly propagating Airy beams [12, 13]—have found use in several applications only a few years since their first realization. For example, Airy beams have been useful in optical micro-manipulation [14], and Airy pulses have been used in inducing filaments and curved plasma channels [15, 16] and have also been applied for micromachining along curved trajectories [17].

In general, the propagation of ultrashort pulses is a spatiotemporal phenomenon, and very often, the electric field of an ultrashort pulse cannot be separated into a product of purely temporal and spatial factors (see, e.g. review [18]). Further, the propagation of an ultrashort pulse through a simple circular aperture creates a separate trailing pulse, which has an X-like spatiotemporal structure and can have almost the same axial

intensity as the main pulse [19, 20, VI]. This can be easily understood in the framework of the boundary diffraction wave theory [19, 21–26], which formulates the diffracted field as a sum of the main and boundary wave contributions. The pulse corresponding to the boundary wave contribution is found to be in the shape of an expanding spindle torus originating from the edge of the aperture and forms an ultrashort counterpart of the well-known Arago spot, which is actually a quasi non-diffractive accelerating Bessel pulse [19, VI].

Although the separability of the pulsed wavefield into temporal and spatial parts may seem convenient, this restriction overlooks the wide variety of spatiotemporally coupled pulses, which have been found useful in many applications. For example, widely used pulse compressors exploit probably the best known spatiotemporal coupling, the angular dispersion [27, 28]. Spatiotemporally coupled pulses can be used to suppress both the spatial and temporal spread of localized light pluses propagating in a bulk dispersive medium [29], and spatiotemporal couplings have an important role in the self-compression of ultrashort laser pulses by filamentation [30, 31]. Additionally, spatiotemporally coupled intense ultrashort pulses have been recently proven to be advantageous for generating isolated attosecond pulses by exploiting the so-called attosecond lighthouse effect [32, 33]. However, in order to introduce spatiotemporal couplings in a controlled manner or avoid them, both the study of non-diffractive waves as well as ultrashort pulse applications in general requires spatiotemporal pulse characterization methods that can accurately and reliably measure the electric field of ultrashort pulses with high spatial and temporal resolutions.

Along with the development of ultrashort sources and their applications, ultrashort pulse measurement methods have evolved as well (see, e.g. reviews [34, 35]). However, the measurement of the shortest events ever created by humans is obviously a rather difficult task since oscilloscopes cannot sample electric field at visible wavelengths. In order to reconstruct the pulse electric field vs. time or, equivalently, the pulse spectrum and spectral phase, the involvement of nonlinear processes and iterative complex retrieval algorithms is needed.

The most common pulse measurement techniques (e.g. FROG [36] and SPIDER [37]) measure the electric field of ultrashort pulses averaged over the cross-section of the beam or in a single point, but our goal is to measure the complete spatiotemporal field in three spatial and one temporal dimension. Although in some cases where the temporal characteristics are uniform over the beam cross-section it is sufficient to measure the pulse at only one point, this is generally not the case for non-diffractive pulsed waves or for spatiotemporally coupled pulses.

The following approach can be adopted to completely characterize the spatiotemporal field of ultrashort pulses. First, a well-characterizable reference pulse is measured. Then, an interferometric or holographic method can be used to measure the spatiotemporal electric field of a complex unknown light pulse with respect to this reference. Furthermore, in many types of experiments, the goal is to characterize the response of an optical device or system, and in that case, the actual employment of temporally coherent femtosecond laser pulses is not obligatory. For example, such methods include digital holography-based STRIPED FISH [38, 39], a variant of spectral interferometry called STARFISH [40], and a variant of spatial spectral interferometry called SEA TADPOLE [41–44]. Recently, the aforementioned interferometric techniques have achieved simultaneous few-micron spatial and few-fs temporal resolutions [45, 46, IX, X]. Further, sub-wavelength spatial resolution has been demonstrated with the SEA TADPOLE technique using near-field scanning microscopy probes [44]. However, the expansion of measurement techniques to sub-cycle accuracy has not yet been accomplished.

In this thesis, the formation and spatiotemporal propagation of ultrabroadband non-diffractive waves is studied with a focus on superluminally propagating Bessel-X pulses, superluminal accelerating and decelerating Bessel pulses, subluminal pulsed Bessel beams, boundary diffraction wave pulses and accelerating Airy pulses. These ultrashort pulsed wavefields are studied both theoretically and experimentally. This thesis remains within the scope of physical optics and scalar description of light in free space or in linear media. The scalar field can be attributed to either linearly polarized electric or magnetic field component of the electromagnetic field.

This thesis is organized as follows.

Section 2 provides an overview of non-diffractive waves. The mathematical formulation and the most common generation methods of Bessel-X pulses, accelerating Bessel pulses, pulsed Bessel beams, and Airy pulses are provided. In addition, the generation of negatively accelerating Bessel pulses owing to diffraction by circular apertures is described, and the expression for a diffracted Gaussian pulse is derived within the framework of boundary diffraction wave theory. Beyond a literature review, this section also contains an overview of the author's original contribution to the theory.

Section 3 gives an overview of interferometric spatiotemporal ultrashort pulse characterization techniques. Both spectral and spatial spectral interferometry setups are considered. The SEA TADPOLE variant of spatial spectral interferometry is covered in greater detail, and the challenges in obtaining ultrabroadband operation of the measurement method are discussed. In addition, specific solutions for these challenges taken in the course of this work are outlined in this section.

Section 4 describes the actual measurement setup and presents the experimental results obtained with SEA TADPOLE on diffracting and non-diffractive light pulses. The measured wavefields are analysed and compared with the theoretical predictions.

Finally, the work is summarized and the main results are outlined on the basis of the author's contribution.

2. DIFFRACTIVE AND NON-DIFFRACTIVE LIGHT PULSES

Localized waves or non-diffractive waves are both spatially and temporally sharply peaked wave packets that propagate seemingly unaffected by diffraction and dispersion. Of course, all of the solutions to the wave equation are prone to diffraction and dispersion. However, in the special case of non-diffractive waves, the wavefield retains its spatial profile within the propagation range thanks to the special angular arrangement of its plane wave constituents and wide aperture. Considering the terminology, the term "non-diffracting" refers to pulses that retain their transversal profile over propagation, and the keyword "localized" refers to bullet-like pulses that are propagation invariant, i.e. also impervious to the temporal spread. First started as an exotic subject in mathematical physics that studied the causality and feasibility of localized wave solutions of the wave equation, the realm of non-diffractive light pulses has now become a rather topical subject and a valuable tool in optics and spectroscopy. In 2008, the first collective monograph [1] on the subject was published, and the second one [2] will be published in 2013.

In this section, an overview of the non-diffractive Bessel beams and pulses is given in subsec. 2.1. Surprisingly, the generation of non-diffractive waves can occur owing to diffraction itself. This is best understood in the framework of the boundary diffraction wave theory, which is discussed in subsec. 2.2. The youngest among the non-diffractive waves—Airy beams—are considered in subsec. 2.3.

2.1. Bessel-type waves

Bessel beams are probably the most well-known "non-diffractive" solutions to the wave equation [3, 4]. The field of a monochromatic Bessel beam can be expressed in cylindrical coordinates as

$$\Psi_B(\rho, \varphi, z) \propto J_n(k_\rho \rho) \exp(\pm \mathrm{i} n \varphi) \exp(\mathrm{i} k_z z), \tag{2.1}$$

where J_n is the nth-order Bessel function of the first kind, k_ρ and k_z are the radial and longitudinal wavevector components, respectively, with $k^2 = k_z^2 + k_\rho^2$ and $k = \omega/c = 2\pi/\lambda$ is the wavenumber of the electromagnetic radiation [47]. The parameter $\theta = \operatorname{atan}(k_\rho/k_z)$ is referred to as the cone angle or the axicon angle of the Bessel beam. An ideal Bessel beam would require infinite aperture and would carry infinite power and is therefore physically impossible to generate as is an ideal plane wave. However, one can generate a quasi-Bessel beam that propagates in a non-diffractive

manner over a finite distance [4]. This distance is called the Bessel zone. As the k-vectors of the Bessel beam lie on a cone, the propagation distance can be geometrically estimated as $z_B = R/\tan\theta$, where R is the radius of the beam.

There are various linear methods for generating Bessel beams: the most common ones are an annular slit in conjunction with a collimating lens, a conical lens (refractive axicon), a reflective axicon and a planar circular diffraction grating (diffractive axicon) (see, e.g. review [48]). In the monochromatic case, the output fields of different Bessel generators are indistinguishable. However, this is not the case for polychromatic or ultrashort illumination, and the properties of the resulting Bessel field are dependent on the generation method. For example, a refractive axicon generates a superluminal Bessel-X pulse, whilst a diffractive axicon generates a subluminal pulsed Bessel beam [49].

2.1.1. Bessel-X pulses

A Bessel-X pulse can be thought of as a cylindrically symmetric angular summation of pairs of plane wave pulses [5] forming a double conical profile. Among localized waves, Bessel-X pulses are probably the most widely studied [5, 29, 50–53, I]. They propagate without exhibiting any spatial or temporal spread in vacuum or linear media over large distances. For example, Bessel pulses have been applied in plasma generation [51, 54], light filamentation [55], imaging [8], micromachining [9, 10], and cell transfection [11]. In addition, Bessel wavepackets have been used to generate optical analogues of the Hawking radiation [6, 7] and to demonstrate the generation of negative frequencies in the process of soliton phase matching [56].

The field of a Bessel-X pulse can be expressed in spectral representation as

$$\Psi_{BX}(\rho, z, t) \propto \int_0^\infty \mathrm{d}\omega S(\omega) J_0(k_\rho \rho) \exp\left[\mathrm{i}\left(k_z z - \omega t\right)\right], \qquad (2.2)$$

where $S(\omega)$ is the spectral amplitude of the pulse [5, 57]. In the case of Bessel-X pulses, the axicon angle θ is constant over the spectrum and the radial wavenumber is proportional to the wavenumber $k_\rho = k\sin\theta$, as is the longitudinal wavenumber $k_z = k\cos\theta$. The propagation speed of the pulse along the z-axis $v_g = c/\cos\theta$ is superluminal, which has been verified by several experiments [5, 29, 50–52] and more recently by direct spatiotemporal measurements [53, I]. Bessel-X pulses can be formed by an annular slit and a collimating achromatic lens, by a reflective axicon or by a refractive axicon, as shown in Fig. 2.1. The variation of the angle θ owing to the dispersion of the axicon material may be neglected even for femtosecond pulses having a bandwidth of up to 40 nm [I].

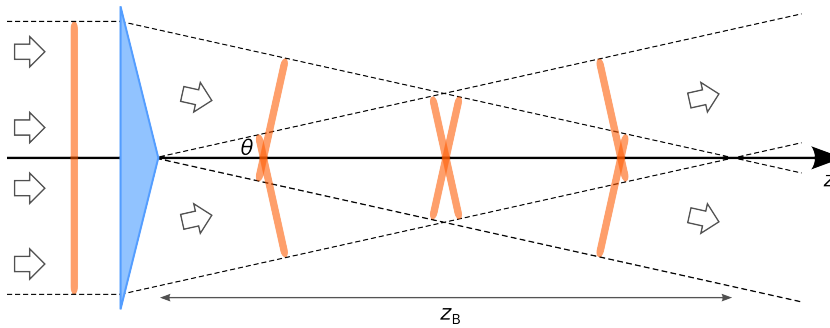

Figure 2.1. Schematic of the formation of a Bessel-X pulse in the case of illumination of a conical lens (axicon) with ultrashort pulses. z_B indicates the range along the propagation axis, where the pulse can be considered "diffraction-free" [V].

2.1.2. Accelerating Bessel pulses

If a lens is placed in front of an axicon, as shown in Fig. 2.2, the plane waves forming a double conical profile of the Bessel-X pulses are replaced by slightly spherical ones. In this case, the axial region of the resulting pulse acquires the shape of a shrinking or expanding spindle torus if the lens is convex or concave, respectively. However, the central spot of these pulses is still localized and intense over a propagation distance considerably longer than that of a Gaussian beam with a comparable waist size. Equation (2.2) can still be used to describe the pulse in the axial region, but the axicon angle θ is not a constant; instead, it is dependent on the propagation distance z as $\theta(z) = \operatorname{atan}\left[\left|f(f-z)^{-1}\right| \tan\theta_0\right]$ [II]. Here, f is the focal length of the lens and θ_0 is the axicon angle of the Bessel field without the lens. As the velocity of the pulse $v_g = c/\cos\theta$ is determined by this angle, we can obtain a pulse whose propagation speed along the z-axis is not only superluminal, but also accelerates or decelerates in free space. Such pulses have been named accelerating Bessel pulses [58].

2.1.3. Pulsed Bessel beam

A pulsed Bessel beam is a Bessel pulse whose spectral components share the same radial profile over its propagation length and can be thought of as a thin slice cut from a Bessel beam [49, 59–61]. In contrast to Bessel-X pulses generated by a refractive axicon, the spatiotemporal profile of the pulsed Bessel beam has no X-like section and its group velocity is subluminal. Although the spatial profile of the pulse propagates in a non-diffracting manner, a pulsed Bessel beam is not propagation invariant, as

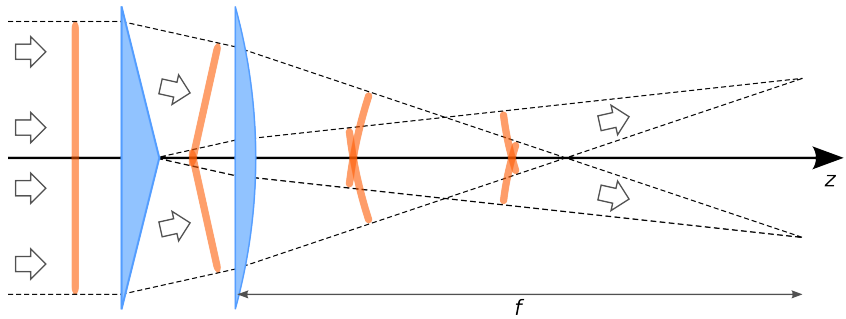

Figure 2.2. Schematic of the formation of accelerating Bessel pulses from a plane-wave pulse. The conical surface of the axicon transforms the plane-wave pulse into a Bessel-X pulse, and the convex lens yields an accelerating pulse [II].

the pulse exhibits spatially induced group-velocity dispersion and broadens temporally over its propagation range in free space.

A pulsed Bessel beam can be generated conveniently with a circularly symmetric binary phase diffraction grating, i.e. diffractive axicon, as shown in Fig. 2.3. If the grating constant is $K = 2\pi/d$, d being the groove spacing, then for a given diffraction order m, the resulting pulsed Bessel beam can be expressed in the form

$$\Psi_{PBB}(\rho, z, t) \propto J_0(k_\rho \rho) \int_0^\infty \mathrm{d}\omega S(\omega) \exp\left[\mathrm{i}\left(k_z z - \omega t\right)\right], \qquad (2.3)$$

where $k_\rho = m \times K$ is the radial wave vector component and $k_z^2 = \omega^2/c^2 - k_\rho^2$ is the longitudinal wave vector component [49, IX]. $S(\omega)$ is the complex spectral amplitude of the pulse taking into account the initial spectrum of the input pulse, initial spectral phase, grating efficiency and on-axis intensity dependence for a monochromatic wave component of the pulsed Bessel beam.

The grating induces negative chirp that may partially compensate for the positive chirp present owing to the material dispersion of the grating substrate and/or propagation medium at certain propagation distances and the pulse is temporally focused. In the region behind the grating where the second-order dispersion effects are balanced, the remaining third-order dispersion sums up and evolves in an unsymmetrical trailing oscillatory temporal envelope, which is confirmed to be a temporal Airy distribution [62]. Therefore, the pulsed Bessel beam temporally focuses into Airy–Bessel wave packets [63, IX].

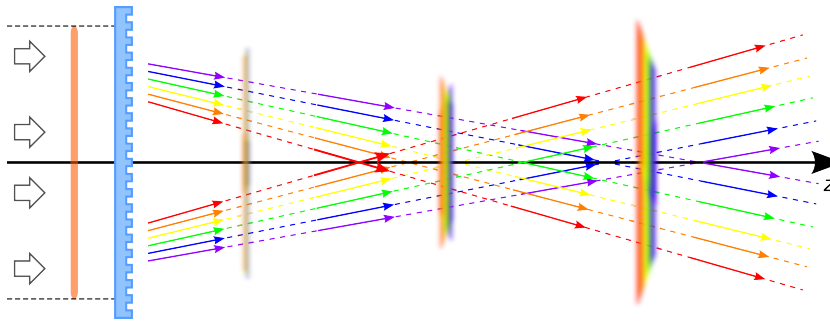

Figure 2.3. Schematic of the formation of a pulsed Bessel beam using a circularly symmetric diffraction grating. The colours represent the different spectral components of an ultrashort pulse and their propagation characteristics. Only one diffraction order is shown.

2.2. Boundary diffraction wave

The diffraction of ultrashort laser pulses is usually studied in the spatial domain at fixed wavelengths. However, in the case of ultrabroadband illumination it may be useful to study the diffraction in the spatiotemporal domain [VI]. The somewhat forgotten and alternative boundary diffraction wave theory has been inspired by the early ideas of Thomas Young and developed by Maggi [21], Rubinowicz [22, 23], Miyamoto and Wolf [24, 25] (see also §8.9 in [26] and Refs. therein). It has been brought into the context of ultrashort laser pulses more recently by Bor and Horváth [19, 20].

The boundary diffraction wave theory treats the diffracted light field as the sum of contributions from geometrical optics and the diffracting aperture. It has been shown to be mathematically equivalent to the well-known Fresnel–Kirchhoff diffraction theory [24, 25]. The contribution from the diffracting aperture or the boundary wave is expressed as a superposition of spherical wavelets emitted from the edge of the diffracting aperture, and its wavefronts form an expanding spindle torus. The main pulse front seems to propagate according to the laws of geometrical optics. In the case of ultrashort pulses, those two contributions often can be separated in time and space, and the boundary diffraction wave formalism thus proves to be a mathematically more simple and intuitive approach to the diffraction phenomena [19, VI]. In terms of boundary diffraction wave theory, the formation of a double pulse behind a diffracting aperture and therefore the modulation of the spectrum of the diffracted ultrashort pulse can be easily understood [20].

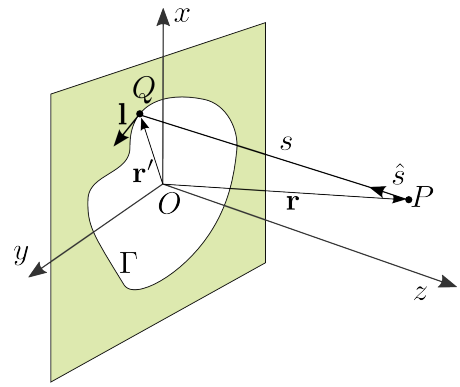

Figure 2.4. Notation relating to the diffraction geometry. P is a point of interest in the half plane behind the diffracting aperture $z > 0$, Q represents a point in the aperture plane, and s is the distance between the points P and Q.

2.2.1. Boundary diffraction wave for plane wave pulses

A mathematical overview of boundary diffraction wave theory is given next. If the diffracting aperture is located at $z = 0$, then according to the boundary diffraction wave theory, the diffracted wave at a point $P = (\rho, \varphi, z)$ in the region $z > 0$ behind the aperture can be represented as a sum of two contributions [25]:

$$U_d(P,\omega) = U_B(P,\omega) + U_G(P,\omega). \tag{2.4}$$

Here, $U_G(P,\omega)$ is a wave that propagates according to the laws of geometrical optics and is called the geometrical wave. It is equal to the incident wave for points in the direct beam and is zero elsewhere. U_B is called the boundary wave and can be expressed by a line integral along the edge of diffracting aperture Γ as

$$U_B(P,\omega) = \oint_\Gamma \mathbf{W}(P,Q,\omega)\,\mathrm{d}\mathbf{l}, \tag{2.5}$$

where $\mathbf{W}$ is a vector potential associated with the incident field $U_i(P,\omega)$, $\mathrm{d}\mathbf{l}$ is the element vector of Γ, and Q represents a point in the aperture plane (see Fig. 2.4). Instead of integration over the area of the diffracting aperture, in the framework of boundary diffraction wave theory, only one-dimensional integration is needed, which may be computationally advantageous.

For an incident monochromatic plane wave, whose propagation direction is determined by a unit vector $\mathbf{p}$:

$$U_i(P,\omega) = A\exp\left(\mathrm{i}\frac{\omega}{c}\mathbf{p}\cdot\mathbf{r}\right), \tag{2.6}$$

where $\mathbf{r}$ is the position vector of point P and A is a constant. In this case, the vector potential in Eq. (2.5) can be expressed as [24]

$$\mathbf{W}(Q,P,\omega)=\frac{A}{4\pi}\exp\left(\mathrm{i}\frac{\omega}{c}\mathbf{p}\cdot\mathbf{r}'\right)\frac{\exp\left(\mathrm{i}\frac{\omega}{c}s\right)}{s}\frac{\hat{s}\times\mathbf{p}}{1+\hat{s}\cdot\mathbf{p}}. \tag{2.7}$$

Here, $\mathbf{r}'$ is the position vector of Q, $\hat{s}$ denotes the unit vector in the direction PQ, i.e. $\hat{s}=\mathbf{s}/s$, and $\mathbf{s}=\mathbf{r}'-\mathbf{r}$.

A polychromatic field can be represented as a superposition of its monochromatic constituents

$$u(P,t)=\mathcal{F}^{-1}\left\{U(P,\omega)\right\}. \tag{2.8}$$

According to the linear properties of the Fourier transform, a diffracted polychromatic field can also be represented as a sum of two contributions, as in Eq. (2.4):

$$u_d(P,t)=u_G(P,t)+u_B(P,t), \tag{2.9}$$

where

$$u_G(P,t)=\mathcal{F}^{-1}\left\{U_G(P,\omega)\right\}, \tag{2.10}$$

$$u_B(P,t)=\mathcal{F}^{-1}\left\{U_B(P,\omega)\right\}. \tag{2.11}$$

Wave fields $u_G(P,t)$ and $u_B(P,t)$ can be considered the main and boundary wave pulses, respectively [19].

Next, the simplest case of a diffraction of a plane wave pulse normally incident on a circular aperture, as shown in Fig. 2.5, will be considered. The incident plane wave pulse can be given as

$$u_i(P,t)=u_0 h\left(t-\frac{z}{c}\right), \tag{2.12}$$

where u_0 is a constant and the function $h(t)=v(t)\exp(-\mathrm{i}\omega_0 t)$ characterises the temporal evolution of the pulse. Here, $v(t)$ represents the temporal envelope function of the pulse and ω_0 is the central frequency. If the aperture radius is a, then the main pulse can be written as

$$u_G(P,t)=\begin{cases}u_i(P,t) & \text{for } \rho<a,\\ 0 & \text{for } \rho>a.\end{cases} \tag{2.13}$$

Equations (2.5), (2.7), and (2.12) can be used to deduce the expression of the boundary wave pulse for the diffracted plane wave [19, 64]:

$$\begin{aligned}u_B(P,t)=&\frac{u_0}{2\pi}\exp(-\mathrm{i}\omega_0 t)\\ &\times\int_0^{\pi}v\left(t-\frac{s(\psi)}{c}\right)\frac{\exp(\mathrm{i}k_0 s(\psi))}{s(\psi)}\frac{a\rho\cos\psi-a^2}{s(\psi)-z}\mathrm{d}\psi.\end{aligned} \tag{2.14}$$

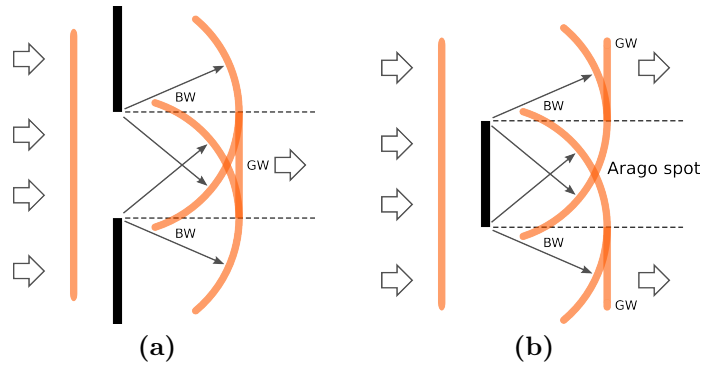

Figure 2.5. Schematic of the formation of a diffraction wave within the framework of boundary diffraction wave theory: (a) behind a circular aperture, (b) behind an opaque disc. The geometrical wave component of the output field is formed directly by the shape of the obstacle. In addition, the edges of the obstacle excite the boundary diffraction wave, which expands from a ring torus shape through a spindle-torus-like stage (cross-section depicted in the figure) into a spherical wave at infinity. On the axis, overlapping and interfering boundary waves form the Arago spot. Around the shadow boundary in the overlap regions of the boundary wave and geometrical wave, the common interference rings appear. In geometry (a), the Arago spot propagates along the axis behind the front of the transmitted geometrical wave, but catches up with the latter at infinity because its velocity is superluminal [VI].

Here, $s(\psi) = \left(z^2 + a^2 + \rho^2 - 2a\rho\cos\psi\right)^{1/2}$ is the distance between the point on the boundary and the point of interest P given in cylindrical coordinates.

From the expression of the boundary wave pulse for the case of a circular aperture given in Eq. (2.14), it can be seen that the boundary wave pulse is simply a sum of spherical wavelets emitted along the edge of the boundary having the temporal profile of the incident pulse and forms a luminally expanding spindle torus [VI]. From Babinet's principle, it follows that the boundary wave pulse in the case of a disc is also given by Eq. (2.14), but with an opposite sign [64]. The formation schematics of the main and boundary wave pulses are shown in Fig. 2.5.

On the optical axis, for $\rho = 0$, the integral in Eq. (2.14) loses its ψ dependence. The diffracted field on the optical axis can therefore be expressed as [19]

$$u(z,t) = u_i(z,t) - A_B(z)\, u_i(z, t - T(z)), \tag{2.15}$$

where $A_B = (1 + z/s_0)/2$, $s_0 = \left(z^2 + a^2\right)^{1/2}$, and $T(z) = (s_0 - z)/c$. Here, A_B represents the relative amplitude of the boundary wave pulse on the optical axis to the incident plane wave. It can be seen from Eq. (2.15)

that on the axis, the boundary wave has the same temporal profile as the incident plane wave. On the plane of the diffracting aperture, the amplitude of the peak of the boundary wave pulse is half of the incident wave and it is delayed with respect to the main pulse by the time it takes light to travel from the edge of the aperture to the optical axis. Further away from the aperture, the boundary wave reaches the same amplitude as the incident plane wave and catches up with it at large distances.

Near the optical axis, it can be shown [19] that the field of the boundary wave pulse can be approximated by

$$u_B(\rho, z, t) \approx -A_B(z)\, u_i(z, t - T(z))\, J_0(k_0 \rho \sin\chi). \tag{2.16}$$

Here, J_0 is the zero order Bessel function of the first kind, and χ is the angle the diffracted ray makes with the optical axis at a particular axial point. Therefore, the boundary diffraction wave pulse can be approximated as a decelerating Bessel pulse [58, II].

2.2.2. Boundary diffraction wave for Gaussian pulses

The boundary diffraction wave formalism was developed first for plane and spherical waves. However, it has been shown by Otis [65, 66] that the boundary diffraction wave theory is also applicable to Gaussian beams—the well-known solution of the paraxial wave equation. This would allow a direct evaluation of the diffracted field of Gaussian pulses in the spatio-temporal domain by a single 1D integration along the diffracting aperture at every point of interest. Compared to the traditional monochromatic treatment of diffraction, the boundary diffraction wave representation may be computationally advantageous in the case of ultrabroadband pulses.

An isodiffracting Gaussian pulse can be written as [67, 68, VII]

$$u_i(\rho, z, t) = \frac{q(0)}{q(z)} v\left(t - \frac{z}{c} - \frac{\rho^2}{2cq(z)}\right) \exp\left[-\mathrm{i}k_0 c\left(t - \frac{z}{c} - \frac{\rho^2}{2cq(z)}\right)\right], \tag{2.17}$$

where

$$v(t) = \exp\left(-4\ln 2 \frac{t^2}{\tau^2}\right) \tag{2.18}$$

is the temporal envelope of the pulse and τ is the pulse duration (FWHM of the field strength). $q(z) = z + d - \mathrm{i}z_R$ is the complex beam parameter, and $z_R = k_0 w_0^2/2$ is the Rayleigh diffraction length, with $z = -d$ as the location of the waist of the smallest spot size w_0 for the central wavenumber k_0. In order to develop an equation for a diffracted Gaussian pulse, a similar approach as in [19] can be taken, where the boundary diffraction wave theory was developed for plane and spherical wave pulses.

If the Gaussian pulse is normally incident on a circular aperture with a radius a, then the field of the pulse propagating according to the laws of geometrical optics is given by [VII]

$$u_G(P,t) = \begin{cases} u_i(P,t) & \text{for } \rho < \rho_h(z), \\ 0 & \text{for } \rho > \rho_h(z), \end{cases} \tag{2.19}$$

where

$$\rho_h(z) = a\,|q(z)/q(0)| \tag{2.20}$$

determines the shadow boundary. The boundary wave pulse for the same case can be written as

$$u_B(P,t) = \frac{a}{2\pi}\exp\left[-\mathrm{i}k_0\left(ct - \frac{a^2}{2q(0)}\right)\right] \times \int_0^{\pi} v\left(t - \frac{a^2}{2cq(0)} - \frac{s(\psi)}{c}\right)\exp\left(\mathrm{i}k_0 s(\psi)\right) f(\psi)\,\mathrm{d}\psi, \tag{2.21}$$

where

$$f(\psi) = \frac{\rho\left[1 - \frac{a^2}{2q^2(0)}\right]\cos\psi - a\left[1 - \frac{a^2}{2q^2(0)}\right] - \frac{az}{q(0)}}{s(\psi)\left[s(\psi) - \frac{a\rho}{q(0)}\cos\psi + \frac{a^2}{q(0)} - z\left(1 - \frac{a^2}{2q^2(0)}\right)\right]}, \tag{2.22}$$

and $s(\psi) = \left(z^2 + a^2 + \rho^2 - 2a\rho\cos\psi\right)^{1/2}$ [VII]. On the optical axis, the integrand in the equation of the boundary wave pulse is independent of the angle ψ, but becomes quickly oscillating off-axis. However, an adaptive quadrature method can be used for evaluating boundary wave pulse integrands. The results for Gaussian pulses are consistent with the limiting cases of plane and spherical waves, i.e. $w_0 \to \infty$ or $d \to \infty$, respectively [VII].

2.3. Airy pulses

Optical beams and pulses with a transverse spatial profile described by the Airy function—the Airy beams—were introduced to optics by Siviloglou and Christodoulides in 2007 [12, 13]. Since then, they have attracted increasing attention, mostly owing to their remarkable property that the intensity maximum of the beam accelerates laterally in free space.

Airy beams arise from a cubic phase of the spatial Fourier spectrum. Most commonly, Airy beams are generated using a spatial light modulator (SLM), as shown in Fig. 2.6. However, there have been reports of successful generation of Airy beams by means of custom design cylindrical lenses [69], or even aberrations of lenses [70]. In addition to lateral acceleration, which

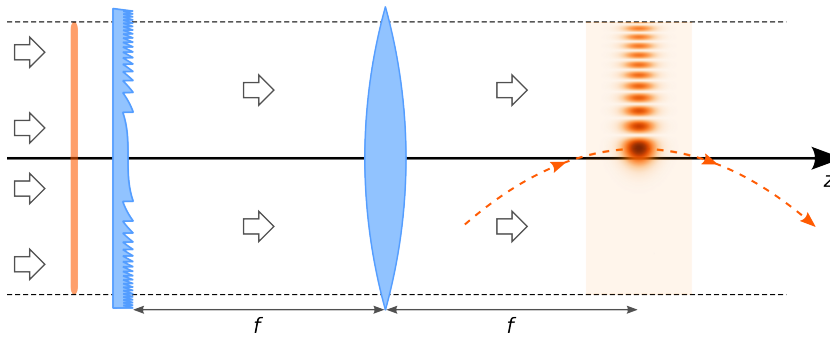

Figure 2.6. Schematic of the formation of an Airy pulse using a cubic phase element and a Fourier transforming lens. The dashed line shows the curved trajectory of the Airy beam maximum.

allows bending of the trajectory of the light maximum around obstacles [71], Airy beams are found to be self-healing, similar to Bessel beams [63, 72].

In addition to the monochromatic Airy fields on which the majority of experiments have been focused, pulsed versions have been introduced [73]. The intense transverse-coordinate-Airy pulses have been used to induce filaments and curved plasma channels in nonlinear regimes [15, 16]. Airy pulses have been applied for micromachining along tailored curved trajectories [17].

The general expression for the wave function of 1D Airy pulses in the paraxial approximation can be given by a superposition of its monochromatic constituents with wavenumber k over spectrum $S(k)$ [73, X]:

$$\Psi(x,z,t) = \int_0^\infty \mathrm{d}k S(k)\, \Phi(x,z,k) \exp\left[ik(z-ct)\right], \tag{2.23}$$

where

$$\begin{aligned}\Phi(x,z,k) =& \mathrm{Ai}\left[\frac{x}{x_0} - \left(\frac{z}{2z_0}\right)^2 + \mathrm{i}a\frac{z}{z_0}\right] \\ &\times \exp\left[a\frac{x}{x_0} - \frac{a}{2}\frac{z^2}{z_0^2} + \mathrm{i}\varphi(x,z,k)\right],\end{aligned} \tag{2.24}$$

and

$$\varphi(x,z,k) = \frac{x}{2x_0}\frac{z}{z_0} - \frac{1}{12}\left(\frac{z}{z_0}\right)^3 + \frac{a^2}{2}\frac{z}{z_0}. \tag{2.25}$$

Here, $\mathrm{Ai}(\dots)$ is the Airy function, x_0 and z_0 are the transversal and longitudinal characteristic lengths, and a is a small positive number to

Table 2.1. Wavenumber dependencies of parameters for four main types of pulses with lateral Airy profile [X].

Type	x_0	z_0	c_0	b_0
I	const.	$\propto k$	$\propto k$	$\propto k^{-2}$
II	$\propto k^{-1}$	$\propto k^{-1}$	const.	$\propto k$
III	$\propto k^{-1/2}$	const.	$\propto k^{1/2}$	$\propto k^{-1/2}$
IV	$\propto k^{-2/3}$	$\propto k^{-1/3}$	$\propto k^{1/3}$	const.

ensure the containment of the infinite Airy trail. However, the parameters x_0 and z_0 are not independent, as the parabolic wave-equation imposes the relation $z_0 = kx_0^2$ on them. Additionally, the parameter $b_0 = x_0/4z_0^2$ characterizes the parabolic trajectory of the main lobe of the Airy beam. Combining two 1D Airy beams for both transverse coordinates, the 2D Airy pulses are obtained: $\Psi(x, y, z, t) = \Psi_x(x, z, t)\,\Psi_y(y, z, t)$.

Airy pulses are most conveniently generated using a cubic phase element on the Fourier plane of a thin lens with a focal length of f (see Fig. 2.6). The Fourier transform of the Airy field at the distance $z = 0$ is given by

$$\Phi_0(\xi, k) = e^{-ac_0^2\xi^2} e^{\mathrm{i}\frac{1}{3}\left(c_0^3\xi^3 - 3a^2c_0\xi - \mathrm{i}a^3\right)}, \tag{2.26}$$

where $c_0 = x_0k/f$ and ξ is the transversal coordinate on the phase element.

The wavenumber dependence of the Airy field parameters x_0, z_0, b_0, and c_0 determines four main types of Airy pulses, which are summarized in Table 2.1 [73, 74]. The first three types are generally applicable to ultrashort pulsed wave fields [73, 75]. Type I Airy pulses have the same spectral distribution in the waist plane $z = 0$. For type II pulses, the spectral distribution is identical in the far field. Type III pulses retain their spectral distribution along the optical axis $x = 0$. In the case of type IV pulses, all the frequency components propagate along the same curved trajectory, so that the main lobe does not disperse [74]. The type of generated Airy pulse is restricted by the generation method used in the particular experimental setup. Thus far, only type II Airy pulses have been experimentally verified [X].

3. SPECTRAL INTERFEROMETRIC ULTRASHORT PULSE CHARACTERIZATION TECHNIQUES

Recent developments in the field of ultrashort pulse generation have made lasers providing few-fs pulses in the visible region available. Along with the development of ultrashort sources and their applications, temporal characterization methods have evolved. Actually, there is a plethora of different measurement techniques (see, e.g. reviews [34, 35]). The intensity autocorrelation, which was the first method for measuring ultrashort pulses, yields some measure of the pulse length, but it is not able to characterize unambiguously the pulse shape [76]. The most prominent methods for measuring the phase and amplitude of the electric field of ultrashort pulses include FROG (Frequency-Resolved Optical Gating) [36] and its variants, e.g. a simplified version of FROG called GRENOUILLE (GRating-Eliminated No-nonsense Observation of Ultrafast Incident Laser Light E-fields) [77], and SPIDER (Spectral-Phase Interferometry for Direct Electric-field Reconstruction) [37]. There are also methods developed more recently, e.g. SRSI [78] and d-scan (d as in dispersion) [79], but these methods have been tested only in the cases of relatively simple pulses. Developing a reliable method for measuring ultrashort pulses is a very complicated task, and even SPIDER, which has been around for 15 years, has recently been found to give erroneous results in some of the common measurement scenarios [80].

All of the aforementioned ultrashort pulse characterization methods measure the electric field at a single point or average over a small fraction of the cross-section of the laser beam. This certainly is not sufficient to accurately measure the spatiotemporally coupled light pulses introduced in the previous section. However, it is possible to use interferometric or holographic methods that are able to measure the electric field of a complex unknown light pulse with respect to a well-characterized reference [81, 82]. Such methods include SEA TADPOLE (Spatially Encoded Arrangement for Temporal Analysis by Dispersing a Pair Of Light E-fields) [41–44], STRIPED FISH (Spatially and Temporally Resolved Intensity and Phase Evaluation Device: Full Information from a Single Hologram) [38, 39], CROAK (Complete Retrieval of the Optical Amplitude and phase using the $(k_\perp, \omega)$ spectrum) [83, 84], Shackled-FROG [53, 85], STARFISH (Spatio-Temporal Amplitude-and-phase Reconstruction by Fourier-transform of Interference Spectra of High-complex-beams) [40] and others. Recently, some of the interferometric methods have achieved measurement of the electric field of complex spatiotemporally coupled pulses with an octave-spanning spectrum [45, 46, IX, X]. It should be noted that for characterizing the

impulse responses of optical devices, neither the measurement of the reference pulse nor the actual employment of coherent femtosecond laser pulses is obligatory.

In this section, several spectral interferometric ultrashort pulse characterization methods that allow high spatial and temporal resolution measurements of ultrabroadband wavefields are considered. Namely, in subsec. 3.1, an overview of spectral interferometry will be given, and in subsec. 3.2, spatial spectral interferometry is considered. In subsec. 3.3, the SEA TADPOLE technique is studied in greater detail.

3.1. Spectral interferometry

Spectral interferometry is a linear method for measuring the ultrashort spectral amplitude and phase responses of optical systems. The main principle of spectral interferometry relies on measuring the combined spectrum of an unknown and a reference pulse, where one of them is delayed with respect to the other. This yields an interference in the frequency domain and the spectral phase of the unknown pulse with respect to the reference pulse can be retrieved [81, 86]. As a linear method, it has been demonstrated in the measurement of very weak pulses [82].

An unknown electric field $E(t)$ at a position $P(x, y, z)$ is given by the convolution of the initial field $E_0(t)$ with the impulse response $h(t)$ of the optical system under characterization $E(t) = E_0(t) * h(t)$. In the frequency domain, the unknown field is $\tilde{E}(\omega) = \tilde{E}_0(\omega) H(\omega)$, where $H(\omega) = F(\omega) \exp(\varphi(\omega))$ is the the complex frequency response of the optical system. If the unknown field is delayed in time by τ, then when those two fields interfere in the spectrometer, the measured spectrum is

$$S_{SI}(\omega) = \left|\tilde{E}(\omega)\right|^2 + \left|\tilde{E}_0(\omega)\right|^2 + 2\left|\tilde{E}(\omega)\right|\left|\tilde{E}_0(\omega)\right| \cos(\omega\tau + \varphi(\omega)). \quad (3.1)$$

By taking a Fourier transform of the measured spectrum and choosing a suitable delay τ, it is possible to separate the interference term in Eq. (3.1) and retrieve the frequency response of the optical system, i.e. the phase and amplitude difference between the reference and unknown fields. The retrieval algorithm is depicted in Fig. 3.1.

Because of the loss in the spectral resolution during the phase retrieval algorithm of the spectral interferometry, the longest pulse measured with the spectral interferometry is often limited [41]. However, it is possible to use a method called phase-stepping spectral interferometry or dual quadrature spectral interferometry, where the spectral interferograms are recorded with four different phase steps: 0, 0.5π, π, and 1.5π. In this case, both the sine and cosine of the phase difference are found. However, it might

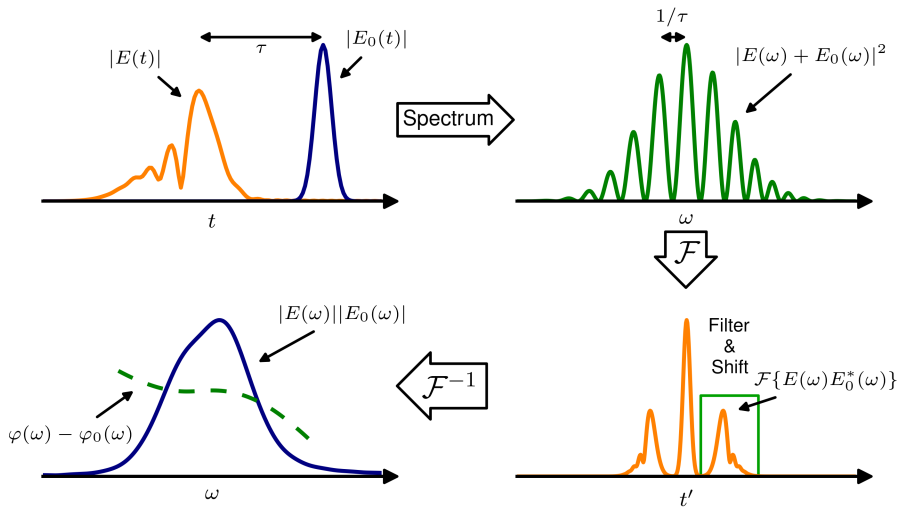

Figure 3.1. Schematic of the trace analysis routine for Fourier-transform spectral interferometry [87].

be experimentally difficult to achieve wavelength-independent and stable phase stepping experimentally [81, 87].

Spectral interferometry has been realized in a fibre-optics-based configuration in a technique called STARFISH [40] that uses a fibre-optic coupler to combine the unknown and reference pulses to be measured with a fibre spectrometer. By scanning the input of the fibre on the measurement arm and recording the interference spectrum at each point of interest, the full spatiotemporal dependence of the field, $E\left(x, y, z, t\right)$, can be easily retrieved.

For example, STARFISH has been used to study circularly symmetric binary amplitude diffraction gratings [88], spatiotemporal evolution of filaments [89], fractal light pulses [90], and ultrashort pulse focusing using a Fresnel lens [91]. The measurement of pulsed light fields as short as 8 fs has been demonstrated using this method [45]. The use of optical fibres in STARFISH has eliminated very precise experimental restrictions on the collimation of the reference and unknown beams otherwise present in the spectral interferometry [41].

3.2. Spatial spectral interferometry

Spatial spectral interferometry [92, 93] is a variation of spectral interferometry that uses non-collinear beams and imaging spectrometer to record a 2D trace. The spectral phase information can be retrieved from interference fringes perpendicular to the frequency axis, and no spectral

resolution is lost during the retrieval. It has also been named by different groups as Spectrally Resolved White Light Interferometry (SRWLI) and Spatially and Spectrally Resolved Interference (SSRI) (see reviews [94, 95] and Refs. therein). Spatial spectral interferometry has emerged as a powerful technique for measuring the phase function of optical elements with high precision [94]. In conjunction with a supercontinuum laser source, it has been recently used for spectral phase measurements of small-scale ($\sim 50\,\mu$m) metamaterial arrays in the infrared region [96].

A variant of spatial spectral interferometry that employs equal length single-mode fibres on the both arms of the interferometer is called SEA TADPOLE [41]. The SEA TADPOLE will be discussed in detail in the next subsection.

Analogous to spectral interferometry, if we consider the fields of two spatially uniform pulses that enter an imaging spectrometer on a small angle θ : $\tilde{E}_0(\omega)\exp\left(\mathrm{i}\frac{\omega}{c}\sin\theta\cdot\xi\right)$ and $\tilde{E}(\omega)\exp\left(-\mathrm{i}\frac{\omega}{c}\sin\theta\cdot\xi\right)$, then the recorded intensity trace on the output plane of the spectrograph reads

$$\begin{aligned} S_{SSI}(\omega,\xi) &= \left|\tilde{E}(\omega)\right|^2 + \left|\tilde{E}_0(\omega)\right|^2 \\ &\quad + 2\left|\tilde{E}(\omega)\right|\left|\tilde{E}_0(\omega)\right|\cos\left(\varphi(\omega) + 2\frac{\omega}{c}\sin\theta\cdot\xi\right), \end{aligned} \tag{3.2}$$

where ξ is the coordinate perpendicular to the frequency on the 2D detector trace. The spatial spectral interferogram in Eq. (3.2) itself provides a fast qualitative feedback about the measured field [93]. Quantitative measurement data can be obtained from the interferogram either by direct cosine fitting [92] or using fast Fourier processing [41]. The latter is found to be three to four times faster than fitting algorithms; however, the cosine fit method is more accurate if the number of fringes is low and the pulses used in the experiment are close to Gaussian [94].

In the following, the Fourier processing of the spatial spectral interferogram is discussed in more detail. By taking the Fourier transform of Eq. (3.2) along the camera coordinate ξ, one can separate the data into three bands:

$$\begin{aligned} S_{SSI}(\omega,\zeta) &= \mathcal{F}\{S_{SSI}(\omega,\xi)\} \\ &= \left|\tilde{E}(\omega)\right|^2\delta(\zeta) + \left|\tilde{E}_0(\omega)\right|^2\delta(\zeta) \\ &\quad + \left|\tilde{E}(\omega)\right|\left|\tilde{E}_0(\omega)\right|e^{-i\varphi(\omega)}\delta\left(\zeta + 2\frac{\omega}{c}\sin\theta\right) \\ &\quad + \left|\tilde{E}(\omega)\right|\left|\tilde{E}_0(\omega)\right|e^{i\varphi(\omega)}\delta\left(\zeta - 2\frac{\omega}{c}\sin\theta\right), \end{aligned} \tag{3.3}$$

where $\delta(\zeta)$ is the Dirac delta function. The required information can be extracted from either of the complex conjugate sidebands. This process is

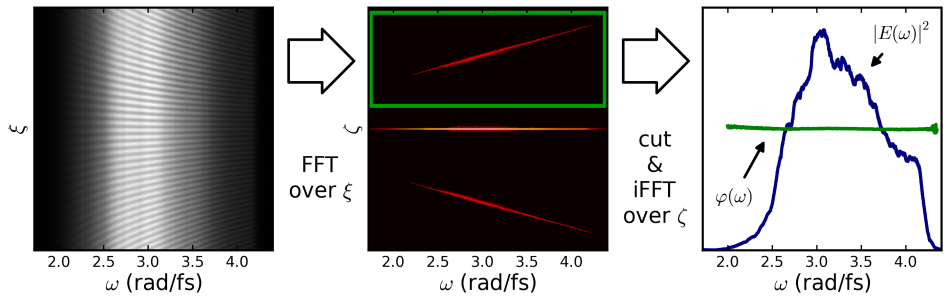

Figure 3.2. Schematic of the trace analysis routine for spatial spectral interferometry [43]. Left: typical spatial spectral interferometry trace. Centre: the magnitude of the Fourier transform of the trace. Right: measurement result obtained from the Fourier filtered trace.

illustrated in Fig. 3.2. As the fringe spacing along the camera coordinate ξ is frequency-dependent and the sidebands are tilted, it is computationally more convenient to inverse-Fourier transform the filtered Eq. (3.3) back to the ξ domain. This tilt then becomes a small linear spectral phase term, $2\frac{\omega}{c}\sin\theta \cdot \xi'$, which usually can be neglected [43]. The linear spectral phase corresponds to a shift in the temporal axis, but it will be the same for all measurements with a given device. In addition, the temporal origin is determined by the path difference between the two arms and is freely adjustable within the temporal measurement range of the device by selecting the delay on the reference arm. Therefore, when the objective is to measure pulse velocity and there is no reference available within the measurable wavefield, it is important to keep the lengths of the interferometer arms fixed and move the optical system under study with respect to the input of the spectrometer (cf., e.g. [I, II, VIII, IX], [VI, VII] and [X]).

The accuracy of the spectrometer calibration plays important role in the quality of the results in spatial spectral interferometry as well as in spectral interferometry [97]. The calibration of the spectrometer can be carried out, as with any other fibre spectrometer, with a calibration lamp. However, as pointed out in [IX], the tilt of the sidebands in the Fourier transform of the spatial spectral interferogram in Eq. (3.3) carries frequency calibration information. If the angle between the unknown and reference beams can be considered wavelength independent, the position of the sideband is proportional to the frequency. The angle can be easily determined using a single monochromatic source, e.g. a HeNe laser. This can be particularly useful in the case of ultrabroadband spectrum and is independent of the dispersing element used in the spectrometer.

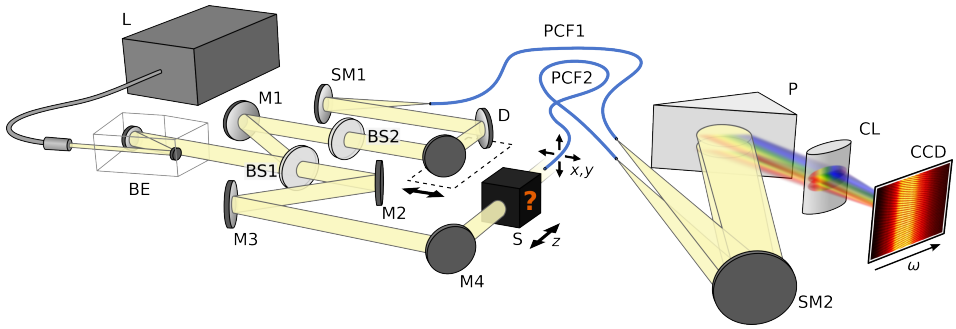

Figure 3.3. Experimental setup for measuring the ultrashort impulse response of an unknown optical system S. The beam from the laser L is expanded by a reflective beam expander BE and then sampled into the reference arm of the interferometer by a UV fused silica window BS1, directed by mirror M1 through a beam splitter dispersion compensation plate BS2 and a variable delay line D, and focused by a spherical mirror SM1 into photonic crystal fibre PCF1. On the measurement arm, the light is directed with mirrors M2–4 to the input of the optical system under measurement S, and the resulting field is sampled by fibre PCF2. The output of the fibres is placed on the entrance slit of an imaging spectrometer with a few mm separation, so that light enters the spectrometer under a small angle 2θ perpendicular to the frequency axis ω. The spectrometer consists of a spherical mirror SM2, reflecting half-prism P, cylindrical lens CL, and a CCD camera. A spatial interference pattern on the CCD camera is processed to retrieve the spectral phase and amplitude information of the field correlation function [IX].

3.3. SEA TADPOLE

SEA TADPOLE is a variant of spatial spectral interferometry that employs equal length single-mode fibres on the both arms of the interferometer. The optical fibres allow effortless redesign of the measurement setup while keeping the most alignment-critical part—the spectrometer—intact. The experimental setup is shown in Fig. 3.3. Scanning the fibre tip on the measurement arm of the interferometers provides the device with a full x, y, z spatial resolution, as the fibres couple light into them only from a small portion of space, which is roughly equal to the mode size of the fibres—typically achieving 3 µm of spatial resolution. Sub-micron spatial resolution has been demonstrated in the SEA TADPOLE setup using near-field scanning microscopy probes [44]. In addition, the fibres can have a useful role as attenuators in balancing the intensities of the signal and reference pulses to optimize the fringe contrast [41]. In the case of ultrabroadband illumination, photonic crystal fibres are required to ensure single-mode operation over the entire spectrum [IX].

The method was first developed for measuring only temporally shaped pulses [41]. However, the capabilities of the SEA TADPOLE in directly characterizing the spatiotemporal electric field $E(x, y, z, t)$ proved to be useful for studying the focusing of ultrashort pulses and aberrations of lenses [42, 44]. SEA TADPOLE has been widely used in measuring ultrashort non-diffractive waves: Bessel-X pulses [I], accelerating Bessel pulses [II], pulsed Bessel beams [VIII, IX], and Airy pulses [X]. It has also been used to study the diffraction of ultrashort pulses and to validate the boundary diffraction wave theory by direct measurements [VI, VII]. Of course, SEA TADPOLE has been applied in measuring shaped pulses [98–100] and found to be useful for characterizing pulse compressors [101]. In addition, there has been some effort for enabling single-shot attosecond measurements using SEA TADPOLE [102]. A method that expands the SEA TADPOLE temporal range by making multiple measurement with different delays has been called MUD TADPOLE (MUltiple Delay for Temporal Analysis by Dispersing a Pair Of Light E-fields) [103, 104].

Much like in any other interferometric pulse characterization technique, the spectrum of the unknown field must be contained within the reference spectrum [41]. The use of optical fibres in SEA TADPOLE can cause slow drift in time in the measured absolute spectral phase [41, 42]. However, this can be simply minimized by enclosing the interferometer. In addition, it has been shown that the absolute phase is actually contained in the measured SEA TADPOLE data, and it can be recovered using a Gerchberg-Saxton-like phase-diversity algorithm, enabling truly complete spatiotemporal measurement of the pulse field [105].

4. RESULTS AND DISCUSSION

In the previous two sections, the overview of several diffractive and non-diffractive light pulses, as well as a few interferometric ultrashort pulse characterization methods was given. In this section, the results obtained from SEA TADPOLE measurements of Bessel-X, accelerating Bessel pulses, pulsed Bessel beams, ultrashort pulse diffraction, and Airy pulses are presented.

The experimental results presented in [I–VIII] were obtained in collaboration with prof. Rick Trebino and then-PhD student Pamela Bowlan at Georgia Institute of Technology, Atlanta, Georgia, USA. As a laser source, a KMLabs Ti:Sapphire oscillator with a ~ 37 nm of bandwidth and ~ 30 fs of pulse duration and a centre wavelength at 805 nm was used. The laser pulses, which served as a reference in these experiments, were routinely monitored using a Swamp Optics GRENOUILLE [41]. The spectrometer in the SEA TADPOLE was calibrated in the near-infrared region over 200 nm centred at the laser wavelength and used a diffraction grating as a diffractive element. In these measurements, a temporal resolution of ~ 17 fs was achieved, and zero filling decreased the point spacing to 4.6 fs [I]. The setup included two solid single-mode fibres with a pure silica core of diameter 5 µm, resulting in a spatial resolution of ~ 3 µm. The detailed description of this particular SEA TADPOLE device can be found in [42, 43, 64].

The experimental results presented in [IX, X] were obtained at the Institute of Physics, University of Tartu, Estonia. For these measurements, the SEA TADPOLE method was further developed to be used together with a ultrabroadband light source to measure the ultrashort impulse responses of optical systems with a spectrum spanning the visible region. A supercontinuum fibre laser Fianum SC-400-2-PP with a spectrum spanning 400–2500 nm was used as a laser source. To ensure single-mode operation of the fibres in the interferometer, photonic crystal fibres were used [106]. Particularly, NKT Photonics LMA-5 was used in [X], and its polarization maintaining version LMA-PM-5 was used in [IX]. The mode field diameter of the fibres is almost constant over the spectrum and has respective values of 4.5 µm and 4.2 µm at 532 nm ($1/e^2$). A prism was used in the spectrometer part of the setup, and the spectral phase and amplitude response was measurable in the range of 428 to 1088 nm. The spectral range was limited by the increasing dispersion of the prism in the blue end and by the diminishing quantum efficiency of Si-based CCD camera in the infrared region. A temporal resolution of up to 2.5 fs, i.e. almost one optical cycle at the central wavelength, could be achieved in this setup [X]. The longest measurable impulse response is determined by the spectral resolution of the

spectrometer, and in the current setup, it is ~ 3 ps, yielding that pulses with a time-bandwidth product of more than 1500 could be accurately measured [IX].

In the case of such an ultrawide bandwidth, every optical element in the setup becomes a challenge of its own. For example, there are no commercially available beamsplitters that have uniform performance over a bandwidth spanning the visible region. Therefore, high-precision UV fused silica windows were used as beam splitters. They have been put into the beam path at an almost normal incidence to minimize unnecessary wavelength-dependent polarization effects and spatial chirp. Coupling only a small fraction of the light out of the measurement arm has the advantage of allowing the measurement of more loosely focused pulses.

4.1. Bessel-X pulses [I, IV, V]

Several preceding publications have reported experimental studies on the properties of Bessel-X pulses. For example, evidence of the X-like spatial profiles and the superluminal propagation of the Bessel-X field were first demonstrated in [5]. The superluminal speed of Bessel-X pulses has also been measured by observing the ionization front in argon gas owing to the central spot of an intense Bessel-X generated using an axicon and 70 fs pulses [51]. However, to the best of our knowledge, the field of a Bessel-X pulse in the course of its propagation has never been directly measured with simultaneous high spatial and temporal resolutions.

To generate the Bessel-X pulses, a fused silica axicon with an apex angle 176° was used (see Fig. 2.1). This resulted in a corresponding Bessel cone angle of $\theta = 0.92°$. The variation of the cone angle over the bandwidth of the laser source owing to the material dispersion of the axicon was $< 5''$ and therefore negligible. To cancel out the group-delay dispersion introduced at the centre of the axicon, a flat glass window with an equal thickness was placed on the reference arm. There was still a small radially varying group-delay dispersion left in the beam, but considering the large apex angle of the axicon and our bandwidth, this effect was insignificant.

The spot size of the laser beam at the front surface of the axicon was 4 mm. The field was scanned with the fibre transversely in the horizontal axis, and the axicon was displaced to several distances from the fibre input longitudinally to yield the spatiotemporal field, $E(x, z, t)$. Three of our measurements together with corresponding simulation results are shown in Fig. 4.1. These results can be considered "snapshot in flight" images of the Bessel-X pulse. The measurements show good agreement with the numerical simulations.

Note that the central maximum of the pulse has a width of $\sim 20\,\mu$m and remains essentially unchanged in shape over 8 cm of propagation. In

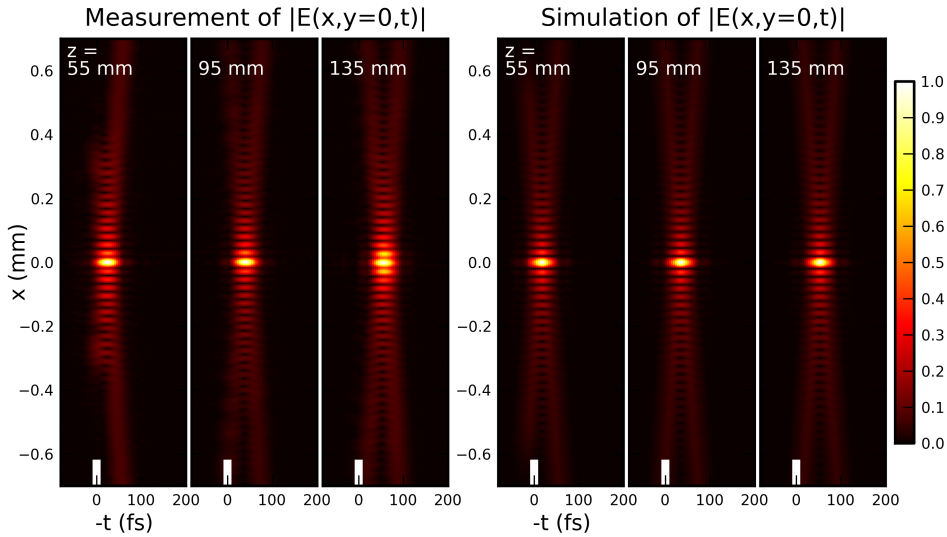

Figure 4.1. Left: the measured field amplitude of the Bessel-X pulse at three different distances after the axicon. Right: the corresponding simulations. The field amplitude is indicated by the colour scale and is normalized for each field. The white bar on the time axis emphasizes the origin of the temporal axis in a reference frame moving at the speed of light [I].

comparison, a Gaussian beam of the same waist would have expanded by 26 times over this distance. As the relative pathlengths of both interferometer arms were kept constant, the recorded temporal positions of the Bessel-X pulse directly reflect its group velocity in a reference frame moving at the speed of light. The superluminal velocity of the pulse is therefore apparent in these plots. The Bessel-X group velocity along the z-axis was found to be $1.00012c$—within 0.001% error of the expected value.

A pulse with both superluminal group and phase velocities may seem intriguing. However, these velocities should not be confused with the signal velocity and do not violate the relativistic causality. Any attempt to cut a signal "notch" into the core of the Bessel-X pulse, would lead the notch to spread out in space luminally. Nevertheless, the central highest-energy part of the Bessel-X pulse propagates rigidly faster than a plane wave, as also seen from the direct measurements.

The results reported in [I] were selected among the most exciting research in 2009 in a special issue of Optics & Photonics News [XV].

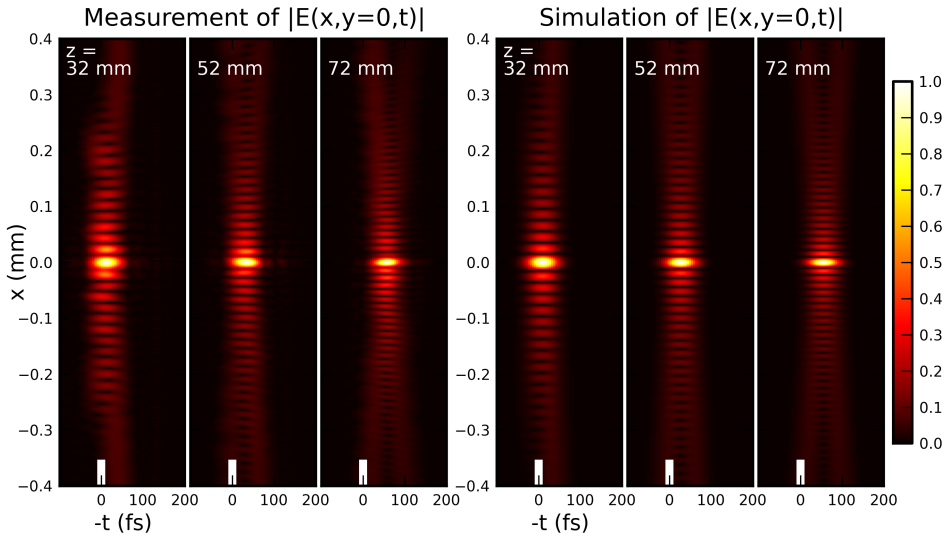

Figure 4.2. Left: the measured spatiotemporal profile of the electric field amplitude of an accelerating Bessel pulse at three positions along the propagation axis. Right: the corresponding simulations [II].

4.2. Accelerating Bessel pulses [II, IV]

To generate accelerating (or decelerating) pulses, a fused silica axicon with an apex angle of 176° was first used to transform plane wave pulses into Bessel-X pulses. Thereafter, lenses with focal lengths of +153 mm and −152 mm were used to transform the Bessel-X pulse into accelerating and decelerating Bessel pulses respectively. For experimental convenience the positions of the axicon and lens were interchanged compared to Fig. 2.2, but this does not influence the results [II]. The spatiotemporal profiles of the pulses were measured at several positions and are shown in comparison with corresponding simulation results in Figs. 4.2 and 4.3. The simulations were performed using Eq. (2.2), taking into account the z-dependence of the axicon angle θ. As seen in the figures, the agreement between the simulations and experimental results is very good.

The group velocity of the accelerating Bessel pulse was measured to accelerate from $1.0002c$ to $1.0009c$ over 4 cm of propagation, and the velocity of the decelerating pulse was measured to decelerate from $1.00007c$ to $100003c$ over a distance of 12 cm. It should be noted that placing a lens in front of the axicon directly compresses or stretches the Bessel zone. Without the lens, the length of the Bessel zone for this axicon was ~ 8 cm; when the positive lens was added (accelerating Bessel pulse), this decreased to ~ 5 cm. In the case of the negative lens (decelerating Bessel pulse), the

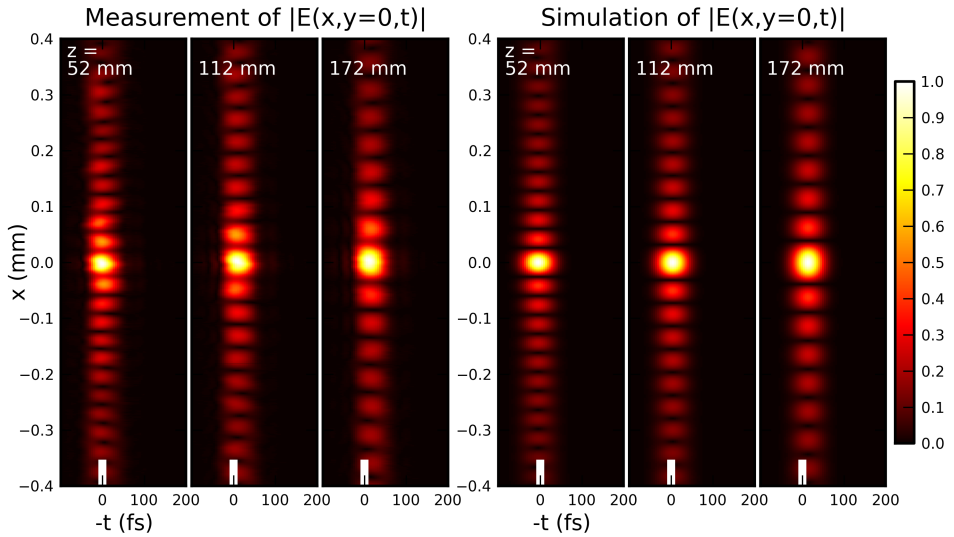

Figure 4.3. Left: the measured spatiotemporal profile of the electric field amplitude of a decelerating Bessel pulse at three positions along the propagation axis. Right: the corresponding simulations [II].

Bessel zone lengthened to tens of kilometres in principle. Despite the fact that we could not measure the pulse kilometres from the axicon, the Bessel ring pattern was observable by eye on the lab wall $\sim 10\,\mathrm{m}$ beyond the axicon.

4.3. Pulsed Bessel beam [VIII, IX]

Pulsed Bessel beams were generated in our experiments using two circularly symmetric binary phase diffraction gratings (diffractive axicons) manufactured at the Heinrich Hertz Institute. The groove spacings of the fused silica diffractive axicons were $d_1 = 100\,\mu\mathrm{m}$ and $d_2 = 20\,\mu\mathrm{m}$, i.e. corresponding to groove densities of $10\,\mathrm{mm}^{-1}$ and $50\,\mathrm{mm}^{-1}$, respectively. The depths of the grating grooves were optimized for a Ti:sapphire laser and were $\delta_1 = 910 \ldots 915\,\mathrm{nm}$ and $\delta_2 = 940 \ldots 945\,\mathrm{nm}$, respectively. The first grating had a duty cycle of 50% and therefore only odd diffraction orders were generated; in the case of the second grating, the duty cycle was 47.5% and weak even diffraction orders were detected.

In Fig. 4.4, the measured spatiotemporal field of the 30 fs laser pulses after passing through the $10\,\mathrm{mm}^{-1}$ circular grating is given at three distances behind the grating. The accompanying simulations are based on the scalar diffraction theory for polychromatic waves. As can be seen in the figure, the grating produces multiple diffraction orders that propagate as a train of

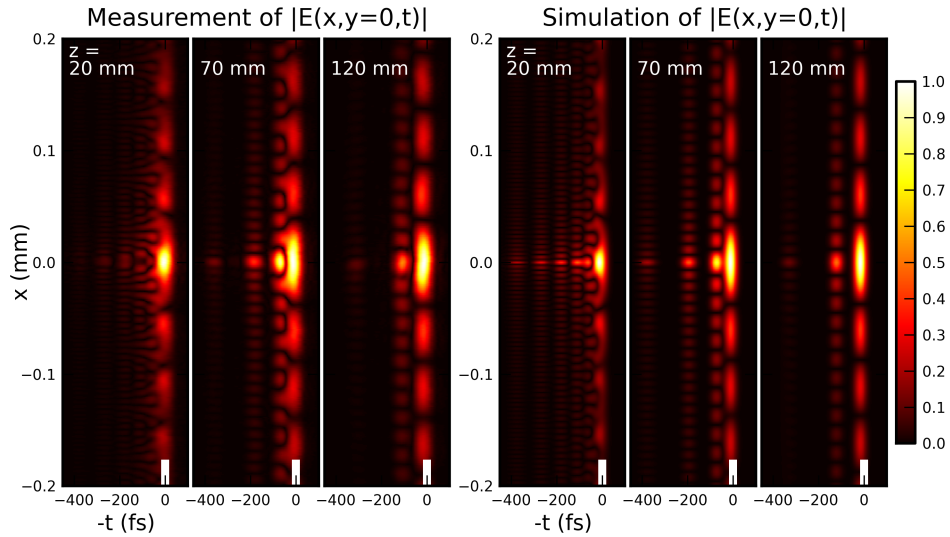

Figure 4.4. Left: the measured spatiotemporal profile of the electric field of an ultrashort pulse diffracted from a circularly symmetric binary phase grating with a groove spacing of $d_1 = 100\,\mu\text{m}$. Right: the corresponding simulations [VIII].

pulses. Each pulsed Bessel beam corresponds to a certain diffraction order. The higher the diffraction order, the lower the subluminal velocities. At a distance of $z = 120\,\text{mm}$, only the first, third, and fifth diffraction orders are present, as the higher orders do not fit inside the temporal window shown. In addition, the higher diffraction orders have shorter propagation lengths as the spectral components of those propagate at higher angles (see also Fig. 2.3).

As described in subsec. 2.1.3, the pulsed Bessel beams are non-diffracting, but not propagation-invariant, as are the Bessel-X pulses. Even in free space they spread out over the course of propagation because of the (negative) dispersion introduced by the grating that increases linearly with the distance. However, in the results presented in Fig. 4.4, this could not be measured because of the very low groove density of the diffraction grating and relatively narrow bandwidth. Therefore, the measurements were repeated with the $50\,\text{mm}^{-1}$ grating using the ultrawideband SEA TADPOLE setup. To test the hypothesis using the diffractive axicon to compensate for material dispersion at certain propagation distances, the measurements were taken with three different amounts of uncompensated dispersion placed in the system. The three cases corresponded to equivalent thicknesses of the fused silica grating substrate: (a) 1.57 mm, i.e. fully uncompensated, (b) 0.92 mm, i.e. partially compensated, and (c) 0 mm, i.e. fully compensated.

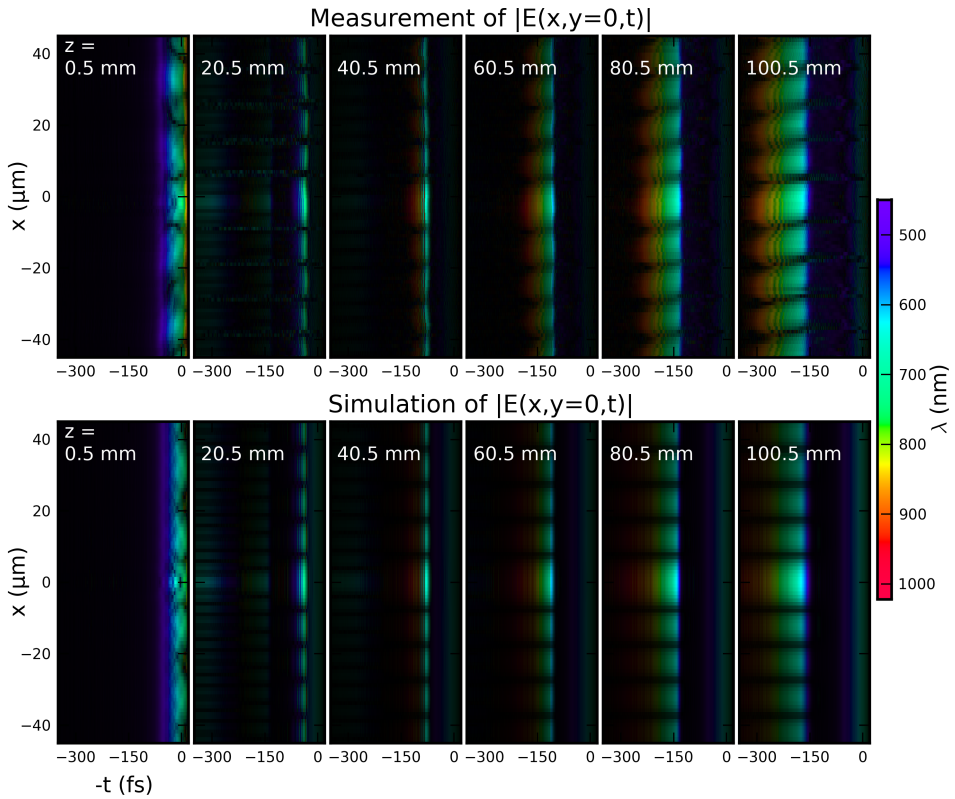

Figure 4.5. Temporal focusing of a pulsed Bessel beam into a Bessel–Airy wave packet generated by a circularly symmetric grating with a groove spacing of $d_2 = 20\,\mu\text{m}$ and a substrate thickness of 0.92 mm. Top: the spatiotemporal measurement; Bottom: the corresponding simulations. Colour shows instantaneous frequency; luminosity shows field amplitude [IX].

The measured impulse response of the partially dispersion compensated diffractive axicon is shown in Fig. 4.5. The simulations were carried out by directly evaluating Eq. (2.3) for the zero to fifth diffraction orders. In addition to previous plots of the spatiotemporal field, in this figure, the instantaneous frequency is shown. It can be seen that a long positively chirped pulse initially focuses in time for certain propagation distances and thereafter spreads out again, becoming negatively chirped. Near the temporal focus, the trailing pulses after the main peak refer to the temporal profile of the Airy–Bessel wave packets. A faint positively chirped pulse corresponding to the zero diffraction order can be seen at greater distances. The theoretical predictions show good agreement with the experimental results.

To further study temporal focusing using the diffractive axicons, the FWHM durations of the pulse intensities were calculated from each measurement. The prevailing first diffraction order with a transform-limited duration of 3.7 fs, which initially after propagation through a 0.92 mm substrate had a duration of 27.8 fs, achieved an average duration of 5.9 fs for propagation distance $z = 20 \ldots 65$ mm with the shortest duration of 5.1 fs. For the fully uncompensated grating substrate, the temporal focusing from 44.8 fs down to an average of 7.0 fs was achieved, and the shortest duration of 6.1 fs occured within the propagation range $z = 40 \ldots 110$ mm. In the case of the fully compensated grating substrate, temporal broadening from 4.1 fs to 91.7 fs was observed over 10 cm of propagation length. Therefore, a 7-fold decrease in the temporal spread of ultrashort pulses was demonstrated at a prescribed propagation depth soley by using this diffractive axicon.

4.4. Boundary diffraction wave [III–VII]

The spatiotemporal field of the diffracted ultrashort pulses was recorded behind four different diffracting apertures: (a) a circular aperture with a diameter of 4.4 mm; (b) an opaque disc with a diameter of 4 mm; (c) an annular slit with a diameter of 5.4 mm and width of 10 µm on a partially transparent substrate; and (d) a system of four concentric annular slits with diameters of 2.1, 4.7, 6.3, and 12.2 mm and widths of 20, 10, 60, and 610 µm, respectively. The measurement results for each case are given in Figs. 4.6, 4.7, 4.8, and 4.9. The simulation results shown in the figures are based on the boundary diffraction wave theory, which was expanded to be applicable to Gaussian pulses. The diffracted field was directly calculated using Eq. (2.9), where the geometric pulse was defined by Eq. (2.19) and the boundary wave pulse was obtained using the adaptive quadrature method to numerically integrate Eq. (2.21). The measurement results were also compared to the boundary diffraction wave theory for plane wave pulses, i.e. the Gaussian pulses from the laser were approximated as plane wave pulses. While this approximation could give good qualitative agreement between the measurement and the theory, the agreement with the simulations based on the diffraction of Gaussian pulses was much better, especially further from the optical axis.

Fig. 4.7 reveals the spatiotemporal structure of the Arago spot—the bright point in the centre of the shadow region, also known as Poisson spot or Fresnel bright spot—which is the fundamental manifestation of the wave nature of light. Interestingly, the plots in Fig. 4.6 reveal the same spatiotemporal structure of the boundary pulse in the diffracted field of the ultrashort pulse behind a circular aperture. Furthermore, the Arago spot appears at the centre any circular boundary, and not only behind a circular

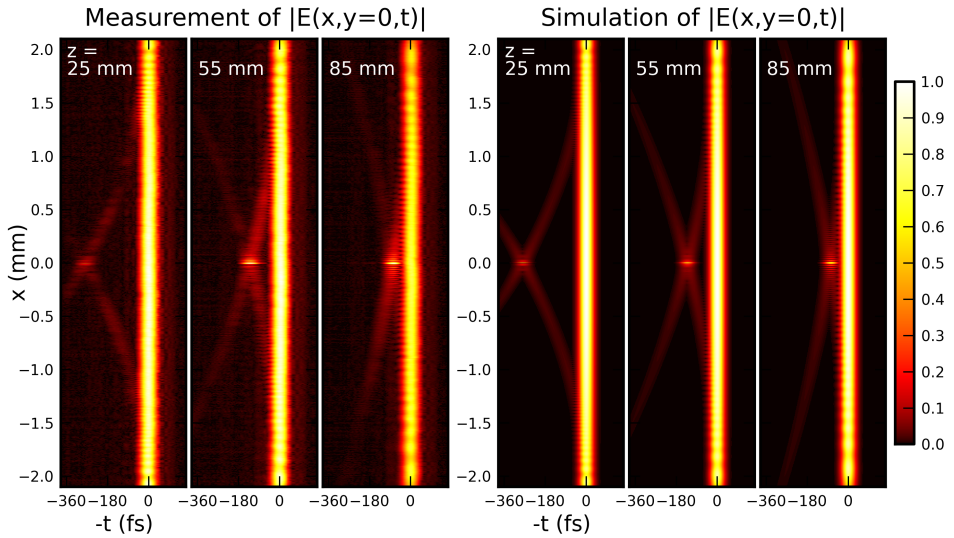

Figure 4.6. Left: the measured light field amplitudes of an ultrashort pulse diffracted by a circular aperture at three distances behind the aperture. Right: the corresponding simulations. The boundary waves interfere with each other and with the directly transmitted pulse, but the interference maximum on the axis (actually a temporally resolved Arago spot) lags behind the direct pulse and eventually catches up with it [VI, VII].

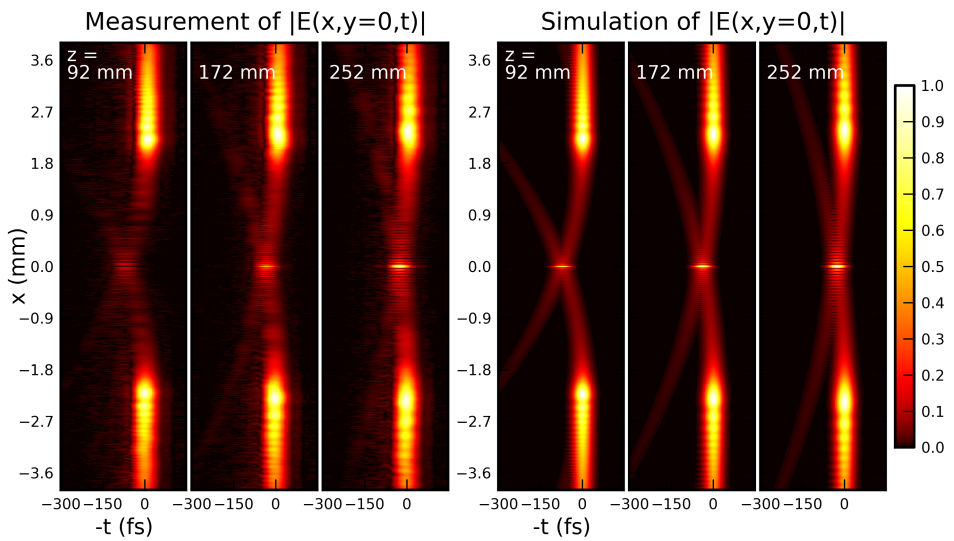

Figure 4.7. Left: the measured propagation and evolution of the diffracted pulse behind an opaque disc. Right: the corresponding simulations. The measurements reveal the spatiotemporal structure of the weak boundary waves and the brightest spot at the centre of the beam owing to their constructive interference, i.e. the Arago spot [VI, VII].

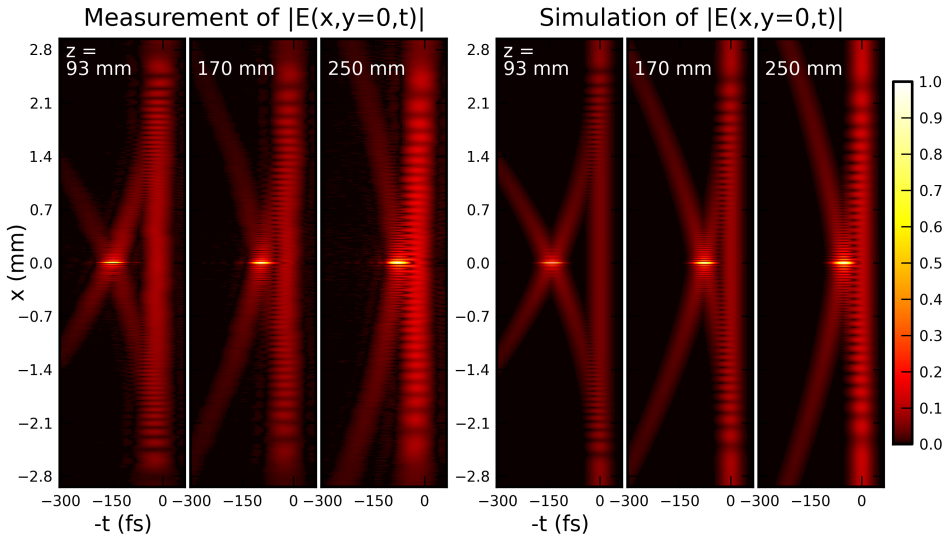

Figure 4.8. Left: the measured electric field amplitude of the pulse generated behind an annular slit on a partially transparent substrate. Right: the corresponding simulations. The partial transmission provided a useful luminally propagating reference pulse, and this series is therefore a good example of the superluminal propagation of the boundary wave pulse [VII].

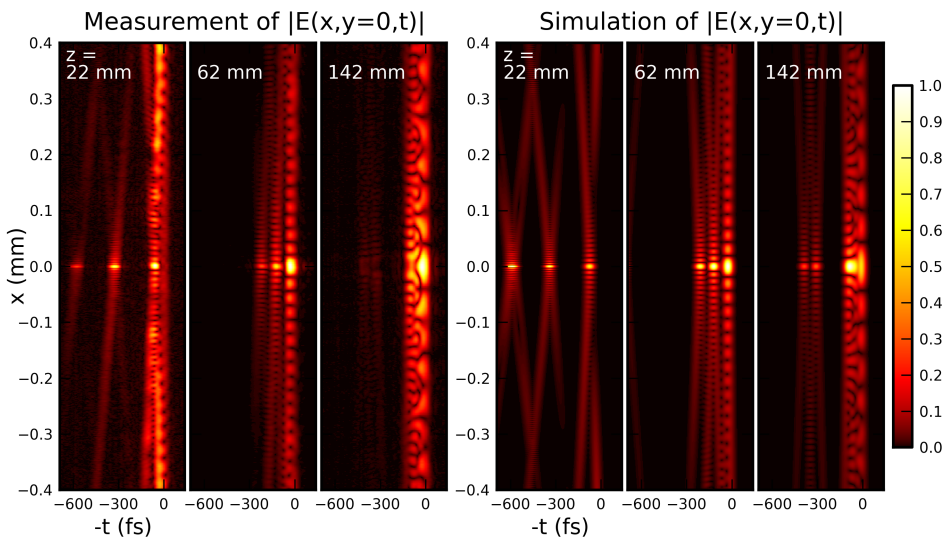

Figure 4.9. Left: the measured electric field amplitude of a pulse diffracted by a system of four concentric annular slits of different widths and diameters. Right: the corresponding simulations. At the distance $z = 142\,\mathrm{mm}$, two separate boundary wave pulses can be resolved that correspond to the inner and outer boundary of the outermost annular slit [VII].

disk. In the case of longer pulses or monochromatic illumination, the boundary wave and the geometric wave overlap, but thanks to the temporal localization of the pulsed illumination and the temporal resolution of our measurements, the small spot can be directly visualized. Therefore, in the case of ultrashort pulses, the boundary diffraction wave theory provides a more intuitive approach to diffraction phenomena in the time domain.

As can be seen in Figs. 4.6 and 4.7, the Arago spot is delayed in time with respect to the main pulse front, and this delay decreases with z, indicating a superluminal propagation speed along the z axis. Indirect observations of this have also been reported previously [20, 107, 108]. In fact, the group velocity of the Arago spot varies from infinity at $z = 0$ to c for very large values of z. As shown in subsec. 2.2, the boundary wave pulse is nothing but a mere decelerating Bessel pulse.

The superluminal propagation of the boundary wave pulse is even more evident in Fig. 4.8, where the partially transparent substrate provides a reference pulse propagating at the speed of light and unaffected by the diffracting aperture. In general, there exists a boundary pulse for both the inner and outer boundary of the annular slit. However, for the most annular slits, those two boundary pulses overlap in time. Two separate pulses can be seen in Fig. 4.9 at $z = 142\,\mathrm{mm}$, corresponding to the outermost annular slit with a width of $610\,\mu\mathrm{m}$. Also, the figure shows how the boundary wave pulses corresponding to slits with different radii are separated in time close to the diffracting aperture and catch up with each other and overlap at larger distances.

The last results show that even more complicated diffraction problems can be understood by rather simple treatments in the time domain. Moreover, the boundary diffraction wave theory aids the general understanding of the diffraction phenomena of ultrashort pulses by expressing the diffracted wavefield as the sum of the boundary and geometric waves. Even quantitatively, all of the setups discussed in this section are calculated by 1D integration from 0 to π at every point of interest. According to the boundary diffraction wave theory, the results are equivalent to Fresnel–Kirchhoff's theory and are not restricted by Fresnel approximations.

The results published in [VII] on the boundary diffraction wave theory for Gaussian pulses and the experiments have been selected into the collection "Highlights of 2012" of the Journal of Optics by the editorial board of the journal.

4.5. Airy pulses [X]

Airy pulses were generated with a reflective liquid-crystal-on-silicon SLM (Holoeye LC-R 2500) with an imprinted wrapped cubic phase mask in

both transverse orthogonal directions. The phase response of the SLM was calibrated using a HeNe laser, and the SLM was placed in the focal plane of an achromatic lens with a focal length of $f = 500\,\mathrm{mm}$, as shown in Fig. 2.6. By measuring the spatially resolved spectral phase along with the intensity, the complete spatiotemporal response function of the Airy pulse generator was reconstructed at various propagation distances. The measured Airy impulse response is shown and compared with simulations in Fig. 4.10. The simulations are based on Eq. (2.23) using the measured spectrum and Airy beam parameters calculated from the phase mask displayed on the SLM. Near the Fourier plane of the lens at the distance $z = 0\,\mathrm{mm}$, the Airy profile is obstructed by the so-called zero order of the SLM. Also considering that in the simulations the laser beam profile was approximated to a Gaussian, the agreement between the measurement and simulations is good.

It was evident from the measured spectral response of the Airy pulse generator that the parabolic deflection rate of the Airy maximum b_0 was proportional to the wavenumber. Consequently, the parameters x_0 and y_0 were proportional to the wavelength, implying that type II Airy pulses were generated in the SLM–lens setup (cf. Table 2.1). Although the phase modulation of the SLM depends greatly on the wavelength, the cubic phase mask on the SLM acted in the same manner over the whole spectrum. The effective phase mask in the current setup was determined rather by the locations of the non-2π phase discontinuities in the phase mask profile than by the obtainable phase modulation depth. Similar wavelength dependence of the Airy beams generated by an SLM has been previously reported in [109], where the propagation properties of Airy beams were studied at four wavelengths. Here, we have done so over a much broader spectral range.

Because of the proportional relationship between the deflection rate and the wavenumber, the measured impulse response exhibited strong lateral dispersion of the pulse maximum, especially near the beginning and end of the measured propagation range. As can be seen in Fig. 4.10, at the furthest distance, the Airy maximum is smeared diagonally. However, it was determined that the temporal duration at the intensity maximum of the measured Airy impulse response remained almost constant near 3.6 fs over the measured propagation range. For the current phase mask, lateral displacement of more than 300 µm over 100 mm of propagation occured.

By measuring the impulse response of a system for shaping ultrabroadband Airy pulses with high spatial and temporal resolution, it was shown that the SLM–lens setup results in type II pulses, which have identical spectral phase distributions over the beam cross-section after the SLM. Aforementioned results are important for the generation of real near single-cycle Airy pulses.

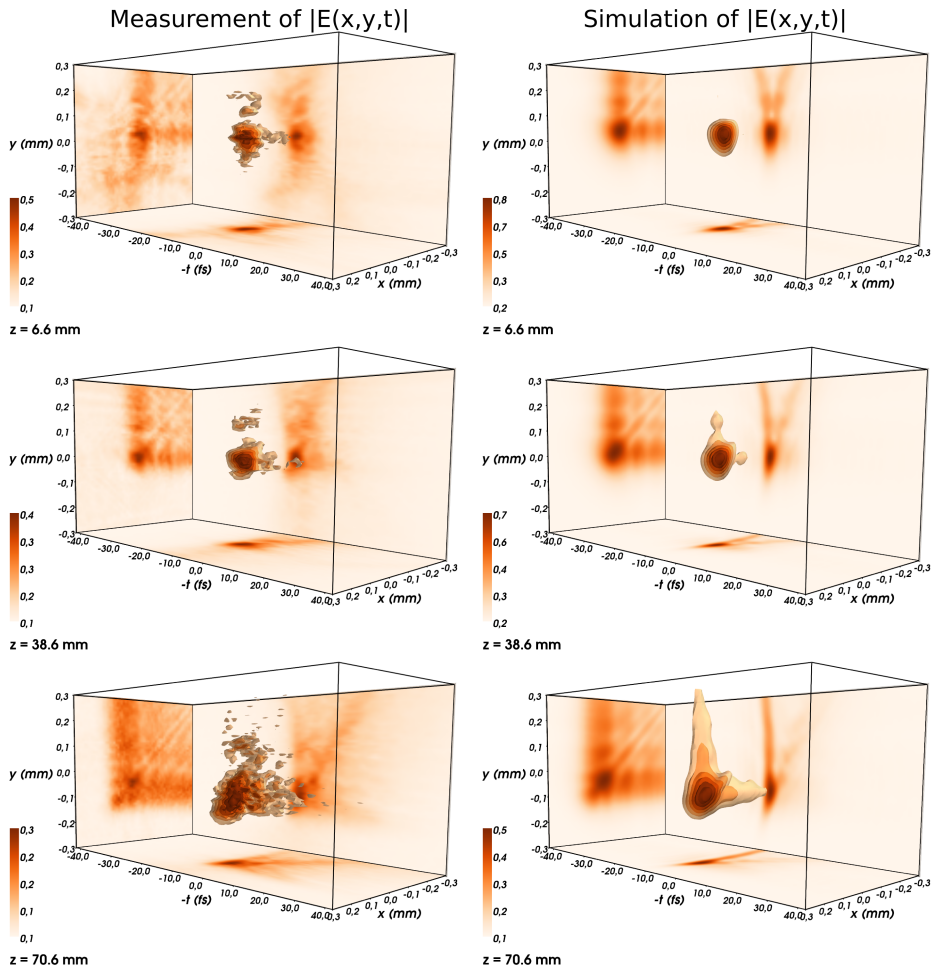

Figure 4.10. Left: the measured impulse response of an SLM–lens Airy pulse generator at three distances. Right: the corresponding simulations. Colour represents the relative amplitude of the electric field. The images show projections of the pulses to the corresponding planes [X].

SUMMARY

This thesis falls within the field of physical optics and more particularly deals with the formation and propagation of ultrabroadband non-diffractive (i.e. localized) waves. These ultrashort pulsed wavefields, whose intensity peaks retains their localization in space and time despite diffraction and dispersion, were studied both theoretically and experimentally. The study included superluminally propagating Bessel-X pulses, superluminal accelerating and decelerating Bessel pulses, subluminal pulsed Bessel beams, boundary diffraction wave pulses and accelerating Airy pulses.

The spatiotemporal characterization of ultrashort pulsed wavefields and impulse responses was carried out using a version of spatial spectral interferometry called SEA TADPOLE that uses equal-length single-mode optical fibres in both arms of the interferometer. The setup was found to be particularly useful for studying the underlying physics of light field transformations in optical systems and for designing and selecting suitable optical elements for generating prescribed ultrashort light fields.

The following main results were obtained:

1. The diffraction of ultrashort Gaussian pulses was studied in the framework of boundary diffraction wave theory. The boundary diffraction wave theory for pulsed wavefields was generalized to apply to Gaussian pulses. An expression for a Gaussian pulse diffracted by a circular boundary was derived, which is evaluable by a one-dimensional integration for every point of interest.

2. The spatiotemporal field of ultrashort Gaussian pulses diffracted by a circular aperture, an opaque disc, an annular slit, and a system of four concentric annular slits was measured using SEA TADPOLE. The formation of superluminally propagating and decelerating boundary wave pulses was directly observed and shown to agree well with theory.

3. A white-light spatial spectral interferometry setup for the characterization of ultrashort impulse responses of optical systems was developed following SEA TADPOLE setup that was adapted for unprecedented octave-spanning spectrum. Using a supercontinuum laser source, a prism-based imaging spectrometer and endlessly single-mode photonic crystal fibres, almost a one-wave-cycle (i.e. 2.5 fs) temporal and 3 µm spatial resolution was achieved in the present realization.

4. The spatiotemporal impulse response of a circularly symmetric binary phase grating, i.e. diffractive axicon generating ultrashort subluminally propagating pulsed Bessel beams was measured using SEA

TADPOLE. The measurements were in good agreement with the simulations.

5. The formation of the Airy–Bessel wave packet behind a diffractive axicon was observed in the spatiotemporal measurements. The temporal focusing of the ultrashort pulse at a prescribed propagation depth was demonstrated, achieving a 7-fold decrease in the temporal spread of the initial pulse using this single optical element.

6. The spatiotemporal impulse response of an optical system for generating ultrabroadband Airy pulses was measured using SEA TADPOLE and was found to be in good agreement with the theory. It was shown that type II Airy pulses are generated in a setup consisting of an SLM with an imprinted wrapped cubic phase and a Fourier transforming lens.

These results from papers [I–X] have been highlighted on the basis of the thesis author's sole or significant contribution (see p. 9). Results from the joint publications that are mainly attributed to the co-authors have not been included in this list.

SUMMARY IN ESTONIAN

Difrageeruvate ja mittedifrageeruvate valgusimpulsside aegruumiline karakteriseerimine

Käesolev doktoritöö kuulub laineoptika valdkonda ja uurib ülilaiaribaliste mittedifrageeruvate ehk lokaliseeritud lainete formeerimist ja levi. Neid ülilühikesi impulsslainevälju, millede intensiivsusmaksimum jääb difraktsioonist ja dispersioonist justkui puutumata ning levib ruumis ja ajas lokaliseeritult ega valgu laiali, on uuritud nii teoreetiliselt kui ka eksperimentaalselt. Töös on käsitletud superluminaalselt levivaid Bessel-X impulsse, superluminaalselt kiirenduvaid kui ka aeglustuvaid Besseli impulsse, subluminaalsed Besseli lainepakette, difraktsiooni äärelaine impulsse ja kiirenduvaid Airy impulsse.

Ülilühikeste impulsslainevälјade ja optiliste süsteemide impulsskosteid mõõdeti ülikõrge ajalise ja ruumilise lahutusega kasutades ruumilis-spektraalsel interferomeetrial põhinevat SEA TADPOLE mõõtemetoodikat, mis kasutab ühepikkusi ühemoodilisi optilisi kiudusid interferomeetri mõlemas õlas. See seade on osutunud väga kasulikuks valgusvälju kujundavate optiliste süsteemide üksikasjalikul uurimisel ning etteantud lainevaljade tekitamiseks sobivate optiliste elementide disainimisel ja valimisel.

Töö põhitulemused on järgnevad.

1. Ülilühikeste Gaussi impulsside difraktsiooni uuriti difraktsiooni äärelaineteooria kontekstis. Ülilühikeste impulsside difraktsiooni äärelaineteooriat üldistati tasa- ja keralaine impulssidelt Gaussi impulssidele. Tuletati avaldis ümmarguselt tõkkelt difrageerunud Gaussi impulsi lainevälja jaoks, mis avaldub ühedimensionaalse integraalina igas huvipakkuvas ruumipunktis.

2. Mõõdeti ümmarguselt avalt, ümmarguselt kettalt, rõngaspilult ja neljast kontsentrilisest rõngaspilust koosnevast süsteemilt difrageerunud ülilühikese Gaussi impulssi laineväli SEA TADPOLE-ga kõrge ajalise ja ruumilise lahutusega. Otseselt õnnestus jälgida ülevalguskiirusel leviva, kuid aeglustuva difraktsiooni äärelaine impulsi ehk tõkke taha tekkiva Arago täpi ajalise analoogi moodustumist ja levikut, mis osutusid teooriaga heas kooskõlas olevateks.

3. Töötati välja valge valguse ruumilis-spetraalse interferomeetria seade optiliste süsteemide ülilühikeste impulsskostete mõõtmiseks ülikõrge ajalise ja ruumilise lahutusega. Seade lähtus SEA TADPOLE mõõteskeemist, mida kohandati töötamaks pretsedenditult laia, üle

ühe oktaavi ulatuva spektriga. Kasutades superkontiinumit genereerivat laserit, kujutavat prismaspektromeetrit ja lõpmatult ühemoodilisi footonkristallist optilisi kiude (*photonic crystal fibres*) saavutati praeguses mõõteseadme realisatsioonis pea-aegu ühele valgusvälja võnkele vastav ehk 2.5 fs ajaline lahutus ja sama-aegne 3 µm ruumiline lahutus.

4. Mõõdeti subluminaalseid Besseli impulsse genereeriva ringsümmeetrilise binaarse faasivõre ehk difrageeriva aksikoni impulsskoste SEA TADPOLE-ga väga kõrge ajalise ja kõrge ruumilise lahutusega. Mõõtetulemused olid heas kooskõlas numbriliste simulatsioonidega.

5. Registreeriti Airy–Bessel valguskuuli teke difrageeriva aksikoni taga. Demonstreeriti ülilühikese impulsi ajalist fokusseerumist etteantud levikukaugusel. Saavutati impulsi kestuse kuni 7-kordne lühenemine võrreldes esialgse, dispersiooni tõttu pikenenud impulsiga, kasutades ainult seda lihtsat optilist elementi.

6. Mõõdeti ülilaiaribaliste Airy impulsside generaatori impulsskoste SEA TADPOLE-ga väga kõrge ajalise ja kõrge ruumilise lahutusega ning mõõtmistulemused leiti olevat heas kooskõlas teooriaga. Õnnestus näidata, et kasutades ruumilisel valgusvälja modulaatoril ja optilist Fourier' pööret sooritaval läätsel põhinevat ülilaiaribaliste Airy impulsside generaatorit, tekivad II tüüpi Airy impulsid, mille puhul valguse spektraalne jaotus on identne kaugväljas.

Eespool mainitud tulemused artiklitest [I–X] on esile tõstetud vastavalt dissertandi panusele tulemuse saavutamisel, mille juures on see olnud ainuisikuline või määrav (vt lk 9). Sellest loetelust on välja jäetud need ühispublikatsioonide tulemused, mille juures on määrav tähtsus olnud kaasautoritel.

ACKNOWLEDGEMENTS

First and foremost, I would like to express my gratitude to my supervisor Prof. Acad. Peeter Saari for his guidance and support throughout the studies and for sharing his invaluable knowledge and expertise.

I greatly acknowledge Prof. Rick Trebino and Dr. Pamela Bowlan for valuable insights into the SEA TADPOLE technique and the ultrashort pulse measurement methods in general.

In addition, I would like to thank all the group members of the Physical Optics Lab at the Institute of Physics, University of Tartu. Especially, I am grateful to Dr. Kaido Reivelt for the supervision in the earlier stages of my studies and to Dr. Heli Lukner for sharing her understanding on the subject of non-diffractive waves and for serving as a good example. I also thank Agu Anijalg for his technical and administrative advice. It has been a pleasure to work together with young colleagues Madis Lõhmus, Ott Rebane, Andreas Valdmann, Roland Matt, and Sandhra-Mirella Valdma in Tartu.

Finally yet importantly, I thank my family and friends for their support, and I am very grateful to my wife Karoliine for her love, understanding and inspiration.

This work has been supported by Estonian Science Foundation grants 6547 and 7870, by Estonian Ministry of Education and Sciences grant SF0180073s07, by Estonian Centre of Excellence in Research "Centre for Nonlinear Studies" receiving funding from the European Regional Development Fund under project 3.2.0101.11-0037 and by graduate school "Functional Materials and Technologies" receiving funding from the European Social Fund under project 1.2.0401.09-0079. This work was carried out in part in the High Performance Computing Centre of the University of Tartu. Financial support from Kristjan Jaak scholarships of the Archimedes Foundation is greatly acknowledged.

REFERENCES

[1] H. E. Hernández-Figueroa, M. Zamboni-Rached, and E. Recami, eds., *Localized Waves* (Wiley, 2008).

[2] H. E. Hernández-Figueroa, M. Zamboni-Rached, and E. Recami, eds., *Nondiffractive Waves* (Wiley, 2013, in press).

[3] J. Durnin, "Exact solutions for nondiffracting beams. I. the scalar theory," J. Opt. Soc. Am. A **4**, 651–654 (1987).

[4] J. Durnin, J. J. Miceli, and J. H. Eberly, "Diffraction-free beams," Phys. Rev. Lett. **58**, 1499–1501 (1987).

[5] P. Saari and K. Reivelt, "Evidence of X-shaped propagation-invariant localized light waves," Phys. Rev. Lett. **79**, 4135–4138 (1997).

[6] F. Belgiorno, S. L. Cacciatori, G. Ortenzi, V. G. Sala, and D. Faccio, "Quantum radiation from superluminal refractive-index perturbations," Phys. Rev. Lett. **104**, 140403 (2010).

[7] E. Rubino, F. Belgiorno, S. L. Cacciatori, M. Clerici, V. Gorini, G. Ortenzi, L. Rizzi, V. G. Sala, M. Kolesik, and D. Faccio, "Experimental evidence of analogue Hawking radiation from ultrashort laser pulse filaments," New J. Phys. **13**, 085005 (2011).

[8] M. Bock, S. K. Das, and R. Grunwald, "Programmable ultrashort-pulsed flying images," Opt. Express **17**, 7465–7478 (2009).

[9] M. K. Bhuyan, F. Courvoisier, P. A. Lacourt, M. Jacquot, R. Salut, L. Furfaro, and J. M. Dudley, "High aspect ratio nanochannel machining using single shot femtosecond Bessel beams," Appl. Phys. Lett. **97**, 081102 (2010).

[10] M. Duocastella and C. Arnold, "Bessel and annular beams for materials processing," Laser Photon. Rev. **6**, 607–621 (2012).

[11] C. T. A. Brown, D. J. Stevenson, X. Tsampoula, C. McDougall, A. A. Lagatsky, W. Sibbett, F. J. Gunn-Moore, and K. Dholakia, "Enhanced operation of femtosecond lasers and applications in cell transfection," J. Biophoton. **1**, 183–199 (2008).

[12] G. A. Siviloglou and D. N. Christodoulides, "Accelerating finite energy Airy beams," Opt. Lett. **32**, 979–981 (2007).

[13] G. A. Siviloglou, J. Broky, A. Dogariu, and D. N. Christodoulides, "Observation of accelerating Airy beams," Phys. Rev. Lett. **99**, 213901 (2007).

[14] J. Baumgartl, M. Mazilu, and K. Dholakia, "Optically mediated particle clearing using airy wavepackets," Nat. Photon. **2**, 675–678 (2008).

[15] P. Polynkin, M. Kolesik, J. V. Moloney, G. A. Siviloglou, and D. N. Christodoulides, "Curved plasma channel generation using ultraintense Airy beams," Science **324**, 229–232 (2009).

[16] P. Panagiotopoulos, D. Abdollahpour, A. Lotti, A. Couairon, D. Faccio, D. G. Papazoglou, and S. Tzortzakis, "Nonlinear propagation dynamics of finite-energy Airy beams," Phys. Rev. A **86**, 013842 (2012).

[17] A. Mathis, F. Courvoisier, L. Froehly, L. Furfaro, M. Jacquot, P. A. Lacourt, and J. M. Dudley, "Micromachining along a curve: Femtosecond laser micromachining of curved profiles in diamond and silicon using accelerating beams," Appl. Phys. Lett. **101**, 071110 (2012).

[18] S. Akturk, X. Gu, P. Bowlan, and R. Trebino, "Spatio-temporal couplings in ultrashort laser pulses," J. Opt. **12**, 093001 (2010).

[19] Z. L. Horváth and Z. Bor, "Diffraction of short pulses with boundary diffraction wave theory," Phys. Rev. E **63**, 026601 (2001).

[20] Z. L. Horváth, J. Klebniczki, G. Kurdi, and A. Kovács, "Experimental investigation of the boundary wave pulse," Opt. Commun. **239**, 243–250 (2004).

[21] G. A. Maggi, "Sulla propagazione libera e perturbata delle onde luminose in mezzo isotropo," Ann. Mat. **16**, 21–48 (1888).

[22] A. Rubinowicz, "Die Beugungswelle in der Kirchhoffschen Theorie der Beugungserscheinungen," Ann. Phys. **358**, 257–278 (1917).

[23] A. Rubinowicz, "Thomas Young and the theory of diffraction," Nature **180**, 160–162 (1958).

[24] K. Miyamoto and E. Wolf, "Generalization of the Maggi–Rubinowicz theory of the boundary diffraction wave—Part I," J. Opt. Soc. Am. **52**, 615–622 (1962).

[25] K. Miyamoto and E. Wolf, "Generalization of the Maggi–Rubinowicz theory of the boundary diffraction wave—Part II," J. Opt. Soc. Am. **52**, 626–636 (1962).

[26] M. Born and E. Wolf, *Principles of optics* (Cambridge University Press, Cambridge, 1999), 7th ed.

[27] E. B. Treacy, "Optical pulse compression with diffraction gratings," IEEE J. Quantum Electron. **5**, 454–458 (1969).

[28] R. L. Fork, O. E. Martinez, and J. P. Gordon, "Negative dispersion using pairs of prisms," Opt. Lett. **9**, 150–152 (1984).

[29] H. Sõnajalg, M. Rätsep, and P. Saari, "Demonstration of the Bessel-X pulse propagating with strong lateral and longitudinal localization in a dispersive medium," Opt. Lett. **22**, 310–312 (1997).

[30] A. Couairon, J. Biegert, C. P. Hauri, W. Kornelis, F. W. Helbing, U. Keller, and A. Mysyrowicz, "Self-compression of ultra-short laser pulses down to one optical cycle by filamentation," J. Mod. Opt. **53**, 75–85 (2006).

[31] A. Mysyrowicz, A. Couairon, and U. Keller, "Self-compression of optical laser pulses by filamentation," New J. Phys. **10**, 025023 (2008).

[32] H. Vincenti and F. Quéré, "Attosecond lighthouses: How to use spatiotemporally coupled light fields to generate isolated attosecond pulses," Phys. Rev. Lett. **108**, 113904 (2012).

[33] J. A. Wheeler, A. Borot, S. Monchocé, H. Vincenti, A. Ricci, A. Malvache, R. Lopez-Martens, and F. Quéré, "Attosecond lighthouses from plasma mirrors," Nat. Photon. **6**, 829–833 (2012).

[34] R. Trebino, P. Bowlan, P. Gabolde, X. Gu, S. Akturk, and M. Kimmel, "Simple devices for measuring complex ultrashort pulses," Laser Photon. Rev. **3**, 314–342 (2009).

[35] I. A. Walmsley and C. Dorrer, "Characterization of ultrashort electromagnetic pulses," Adv. Opt. Photon. **1**, 308–437 (2009).

[36] R. Trebino and D. J. Kane, "Using phase retrieval to measure the intensity and phase of ultrashort pulses: frequency-resolved optical gating," J. Opt. Soc. Am. A **10**, 1101–1111 (1993).

[37] C. Iaconis and I. A. Walmsley, "Spectral phase interferometry for direct electric-field reconstruction of ultrashort optical pulses," Opt. Lett. **23**, 792–794 (1998).

[38] P. Gabolde and R. Trebino, "Single-shot measurement of the full spatio-temporal field of ultrashort pulses with multi-spectral digital holography," Opt. Express **14**, 11460–11467 (2006).

[39] P. Gabolde and R. Trebino, "Single-frame measurement of the complete spatiotemporal intensity and phase of ultrashort laser pulses using wavelength-multiplexed digital holography," J. Opt. Soc. Am. B **25**, A25–A33 (2008).

[40] B. Alonso, Í. J. Sola, Ó. Varela, J. Hernández-Toro, C. Méndez, J. S. Román, A. Zaïr, and L. Roso, "Spatiotemporal amplitude-and-phase reconstruction by Fourier-transform of interference spectra of high-complex-beams," J. Opt. Soc. Am. B **27**, 933–940 (2010).

[41] P. Bowlan, P. Gabolde, A. Shreenath, K. McGresham, R. Trebino, and S. Akturk, "Crossed-beam spectral interferometry: a simple, high-spectral-resolution method for completely characterizing complex ultrashort pulses in real time," Opt. Express **14**, 11892–11900 (2006).

[42] P. Bowlan, P. Gabolde, and R. Trebino, "Directly measuring the spatio-temporal electric field of focusing ultrashort pulses," Opt. Express **15**, 10219–10230 (2007).

[43] P. Bowlan, P. Gabolde, M. A. Coughlan, R. Trebino, and R. J. Levis, "Measuring the spatiotemporal electric field of ultrashort pulses with high spatial and spectral resolution," J. Opt. Soc. Am. B **25**, A81–A92 (2008).

[44] P. Bowlan, U. Fuchs, R. Trebino, and U. D. Zeitner, "Measuring the spatiotemporal electric field of tightly focused ultrashort pulses with sub-micron spatial resolution," Opt. Express **16**, 13663–13675 (2008).

[45] B. Alonso, M. Miranda, Í. J. Sola, and H. Crespo, "Spatiotemporal characterization of few-cycle laser pulses," Opt. Express **20**, 17880–17893 (2012).

[46] B. Alonso, M. Miranda, F. Silva, V. Pervak, J. Rauschenberger, J. San Román, Í. J. Sola, and H. Crespo, "Characterization of sub-two-cycle pulses from a hollow-core fiber compressor in the spatiotemporal and spatiospectral domains," Appl. Phys. B (2013, in press).

[47] A. Vasara, J. Turunen, and A. T. Friberg, "Realization of general nondiffracting beams with computer-generated holograms," J. Opt. Soc. Am. A **6**, 1748–1754 (1989).

[48] D. McGloin and K. Dholakia, "Bessel beams: Diffraction in a new light," Contemp. Phys. **46**, 15–28 (2005).

[49] A. M. Shaarawi and I. M. Besieris, "On the superluminal propagation of X-shaped localized waves," J. Phys. A–Math. Gen. **33**, 7227–7254 (2000).

[50] D. Mugnai, A. Ranfagni, and R. Ruggeri, "Observation of superluminal behaviors in wave propagation," Phys. Rev. Lett. **84**, 4830–4833 (2000).

[51] I. Alexeev, K. Y. Kim, and H. M. Milchberg, "Measurement of the superluminal group velocity of an ultrashort Bessel beam pulse," Phys. Rev. Lett. **88**, 073901 (2002).

[52] R. Grunwald, V. Kebbel, U. Griebner, U. Neumann, A. Kummrow, M. Rini, E. T. J. Nibbering, M. Piché, G. Rousseau, and M. Fortin, "Generation and characterization of spatially and temporally localized few-cycle optical wave packets," Phys. Rev. A **67**, 063820 (2003).

[53] F. Bonaretti, D. Faccio, M. Clerici, J. Biegert, and P. D. Trapani, "Spatiotemporal amplitude and phase retrieval of Bessel-X pulses using a Hartmann-Shack sensor," Opt. Express **17**, 9804–9809 (2009).

[54] P. Polynkin, M. Kolesik, A. Roberts, D. Faccio, P. D. Trapani, and J. Moloney, "Generation of extended plasma channels in air using femtosecond Bessel beams," Opt. Express **16**, 15733–15740 (2008).

[55] P. Polesana, M. Franco, A. Couairon, D. Faccio, and P. Di Trapani, "Filamentation in Kerr media from pulsed Bessel beams," Phys. Rev. A **77**, 043814 (2008).

[56] E. Rubino, J. McLenaghan, S. C. Kehr, F. Belgiorno, D. Townsend, S. Rohr, C. E. Kuklewicz, U. Leonhardt, F. König, and D. Faccio, "Negative-frequency resonant radiation," Phys. Rev. Lett. **108**, 253901 (2012).

[57] P. Saari and H. Sõnajalg, "Pulsed Bessel beams," Laser Phys. **7**, 32–39 (1997).

[58] M. Clerici, D. Faccio, A. Lotti, E. Rubino, O. Jedrkiewicz, J. Biegert, and P. D. Trapani, "Finite-energy, accelerating Bessel pulses," Opt. Express **16**, 19807–19811 (2008).

[59] Z. Liu and D. Fan, "Propagation of pulsed zeroth-order Bessel beams," J. Mod. Opt. **45**, 17–21 (1998).

[60] W. Hu and H. Guo, "Ultrashort pulsed Bessel beams and spatially induced group-velocity dispersion," J. Opt. Soc. Am. A **19**, 49–53 (2002).

[61] M. A. Porras, "Diffraction effects in few-cycle optical pulses," Phys. Rev. E **65**, 026606 (2002).

[62] Z. Ren, H. Jin, Y. Shi, J. Xu, W. Zhou, and H. Wang, "Spatially induced spatiotemporally nonspreading Airy–Bessel wave packets," J. Opt. Soc. Am. A **29**, 848–853 (2012).

[63] A. Chong, W. H. Renninger, D. N. Christodoulides, and F. W. Wise, "Airy–Bessel wave packets as versatile linear light bullets," Nat. Photon. **4**, 103–106 (2010).

[64] P. Piksarv, "Ülilühikesed optilised impulsid difraktsiooni äärelaine-teoorias ja nende eksperimentaalne registreerimine," Master's thesis, University of Tartu (2009). P. Saari, H. Valtna-Lukner and K. Reivelt, sup.

[65] G. Otis, "Application of the boundary-diffraction-wave theory to Gaussian beams," J. Opt. Soc. Am. **64**, 1545–1550 (1974).

[66] G. Otis, J.-L. Lachambre, J. W. Y. Lit, and P. Lavigne, "Diffracted waves in the shadow boundary region," J. Opt. Soc. Am. **67**, 551–553 (1977).

[67] E. Heyman and T. Melamed, "Certain considerations in aperture synthesis of ultrawideband/short-pulse radiation," IEEE T. on Antenn. Propag. **42**, 518–525 (1994).

[68] Z. Wang, Z. Zhang, Z. Xu, and Q. Lin, "Space-time profiles of an ultrashort pulsed Gaussian beam," IEEE J. Quantum Elect. **33**, 566 –573 (1997).

[69] B. Yalizay, B. Soylu, and S. Akturk, "Optical element for generation of accelerating Airy beams," J. Opt. Soc. Am. A **27**, 2344–2346 (2010).

[70] D. Abdollahpour, S. Suntsov, D. G. Papazoglou, and S. Tzortzakis, "Spatiotemporal Airy light bullets in the linear and nonlinear regimes," Phys. Rev. Lett. **105**, 253901 (2010).

[71] G. A. Siviloglou, J. Broky, A. Dogariu, and D. N. Christodoulides, "Ballistic dynamics of Airy beams," Opt. Lett. **33**, 207–209 (2008).

[72] J. Broky, G. A. Siviloglou, A. Dogariu, and D. N. Christodoulides, "Self-healing properties of optical Airy beams," Opt. Express **16**, 12880–12891 (2008).

[73] P. Saari, "Laterally accelerating Airy pulses," Opt. Express **16**, 10303–10308 (2008).

[74] Y. Kaganovsky and E. Heyman, "Airy pulsed beams," J. Opt. Soc. Am. A **28**, 1243–1255 (2011).

[75] C. J. R. Sheppard, "Bessel pulse beams and focus wave modes," J. Opt. Soc. Am. A **18**, 2594–2600 (2001).

[76] R. Trebino, *Frequency-resolved Optical Gating: The Measurement of Ultrashort Laser Pulses* (Kluwer Academic Publishers, 2000).

[77] P. O'Shea, M. Kimmel, X. Gu, and R. Trebino, "Highly simplified device for ultrashort-pulse measurement," Opt. Lett. **26**, 932–934 (2001).

[78] T. Oksenhendler, S. Coudreau, N. Forget, V. Crozatier, S. Grabielle, R. Herzog, O. Gobert, and D. Kaplan, "Self-referenced spectral interferometry," Appl. Phys. B **99**, 7–12 (2010).

[79] M. Miranda, T. Fordell, C. Arnold, A. L'Huillier, and H. Crespo, "Simultaneous compression and characterization of ultrashort laser pulses using chirped mirrors and glass wedges," Opt. Express **20**, 688–697 (2012).

[80] J. Ratner, G. Steinmeyer, T. C. Wong, R. Bartels, and R. Trebino, "Coherent artifact in modern pulse measurements," Opt. Lett. **37**, 2874–2876 (2012).

[81] L. Lepetit, G. Chériaux, and M. Joffre, "Linear techniques of phase measurement by femtosecond spectral interferometry for applications in spectroscopy," J. Opt. Soc. Am. B **12**, 2467–2474 (1995).

[82] D. N. Fittinghoff, J. L. Bowie, J. N. Sweetser, R. T. Jennings, M. A. Krumbüugel, K. W. DeLong, R. Trebino, and I. A. Walmsley, "Measurement of the intensity and phase of ultraweak, ultrashort laser pulses," Opt. Lett. **21**, 884–886 (1996).

[83] F. Bragheri, D. Faccio, F. Bonaretti, A. Lotti, M. Clerici, O. Jedrkiewicz, C. Liberale, S. Henin, L. Tartara, V. Degiorgio, and P. D. Trapani, "Complete retrieval of the field of ultrashort optical pulses using the angle-frequency spectrum," Opt. Lett. **33**, 2952–2954 (2008).

[84] D. Faccio, A. Lotti, A. Matijosius, F. Bragheri, V. Degiorgio, A. Couairon, and P. D. Trapani, "Experimental energy-density flux characterization of ultrashort laser pulse filaments." Opt. Express **17**, 8193–8200 (2009).

[85] E. Rubino, D. Faccio, L. Tartara, P. K. Bates, O. Chalus, M. Clerici, F. Bonaretti, J. Biegert, and P. D. Trapani, "Spatiotemporal amplitude and phase retrieval of space-time coupled ultrashort pulses using the Shackled-FROG technique," Opt. Lett. **34**, 3854–3856 (2009).

[86] C. Froehly, A. Lacourt, and J. C. Viénot, "Time impulse response and time frequency response of optical pupils.:Experimental confirmations and applications," Nouv. Rev. Opt. **4**, 183–196 (1973).

[87] P. Gabolde and P. Bowlan, "Ultrafast interferometry," in "FROG: Ultrafast Optics Textbook," , vol. 1, R. Trebino and J. Squier, eds. (2007), chap. 12. Http://frog.gatech.edu/prose.html.

[88] O. Mendoza-Yero, B. Alonso, O. Varela, G. Mínguez-Vega, Í. J. Sola, J. Lancis, V. Climent, and L. Roso, "Spatio-temporal characterization of ultrashort pulses diffracted by circularly symmetric hard-edge apertures: theory and experiment," Opt. Express **18**, 20900–20911 (2010).

[89] B. Alonso, Í. J. Sola, J. S. Román, Ó. Varela, and L. Roso, "Spatiotemporal evolution of light during propagation in filamentation regime," J. Opt. Soc. Am. B **28**, 1807–1816 (2011).

[90] O. Mendoza-Yero, B. Alonso, G. Mínguez-Vega, Í. J. Sola, J. Lancis, and J. A. Monsoriu, "Synthesis of fractal light pulses by quasi-direct space-to-time pulse shaping," Opt. Lett. **37**, 1145–1147 (2012).

[91] B. Alonso, R. Borrego-Varillas, O. Mendoza-Yero, Í. J. Sola, J. S. Román, G. Mínguez-Vega, and L. Roso, "Frequency resolved wavefront retrieval and dynamics of diffractive focused ultrashort pulses," J. Opt. Soc. Am. B **29**, 1993–2000 (2012).

[92] A. P. Kovács, K. Osvay, Z. Bor, and R. Szipöcs, "Group-delay measurement on laser mirrors by spectrally resolved white-light interferometry," Opt. Lett. **20**, 788–790 (1995).

[93] D. Meshulach, D. Yelin, and Y. Silberberg, "Real-time spatial–spectral interference measurements of ultrashort optical pulses," J. Opt. Soc. Am. B **14**, 2095–2098 (1997).

[94] A. Börzsönyi, A. Kovács, M. Görbe, and K. Osvay, "Advances and limitations of phase dispersion measurement by spectrally and spatially resolved interferometry," Opt. Commun. **281**, 3051–3061 (2008).

[95] A. Börzsönyi, A. P. Kovács, and K. Osvay, "What we can learn about ultrashort pulses by linear optical methods," Appl. Sci. **3**, 515–544 (2013).

[96] K. O'Brien, N. D. Lanzillotti-Kimura, H. Suchowski, B. Kante, Y. Park, X. Yin, and X. Zhang, "Reflective interferometry for optical metamaterial phase measurements," Opt. Lett. **37**, 4089–4091 (2012).

[97] C. Dorrer, "Influence of the calibration of the detector on spectral interferometry," J. Opt. Soc. Am. B **16**, 1160–1168 (1999).

[98] J. J. Field, C. G. Durfee, J. A. Squier, and S. Kane, "Quartic-phase-limited grism-based ultrashort pulse shaper," Opt. Lett. **32**, 3101–3103 (2007).

[99] M. A. Coughlan, M. Plewicki, and R. J. Levis, "Parametric spatio-temporal control of focusing laser pulses," Opt. Express **17**, 15808–15820 (2009).

[100] M. A. Coughlan, M. Plewicki, and R. J. Levis, "Spatio-temporal and -spectral coupling of shaped laser pulses in a focusing geometry," Opt. Express **18**, 23973–23986 (2010).

[101] V. Chauhan, P. Bowlan, J. Cohen, and R. Trebino, "Single-diffraction-grating and grism pulse compressors," J. Opt. Soc. Am. B **27**, 619–624 (2010).

[102] F. Quéré, H. George, and P. Martin, "Attosecond and femtosecond metrology for plasma mirrors," Proc. SPIE **7359**, 73590E (2009).

[103] J. Cohen, P. Bowlan, V. Chauhan, and R. Trebino, "Measuring temporally complex ultrashort pulses using multiple-delay crossed-beam spectral interferometry," Opt. Express **18**, 6583–6597 (2010).

[104] J. Cohen, P. Bowlan, and R. Trebino, "Extending femtosecond metrology to longer, more complex laser pulses in time and space," IEEE J. Sel. Top. Quant. Electron. **18**, 218–227 (2012).

[105] P. Bowlan and R. Trebino, "Using phase diversity for the measurement of the complete spatiotemporal electric field of ultrashort laser pulses," J. Opt. Soc. Am. B **29**, 244–248 (2012).

[106] J. C. Knight, "Photonic crystal fibres," Nature **424**, 847–851 (2003).

[107] D. Chauvat, O. Emile, M. Brunel, and A. L. Floch, "Direct measurement of the central fringe velocity in Young-type experiments," Phys. Lett. A **295**, 78–80 (2002).

[108] M. Vasnetsov, V. Pas'ko, A. Khoroshun, V. Slyusar, and M. Soskin, "Observation of superluminal wave-front propagation at the shadow area behind an opaque disk," Opt. Lett. **32**, 1830–1832 (2007).

[109] J. E. Morris, M. Mazilu, J. Baumgartl, T. Cižmár, and K. Dholakia, "Propagation characteristics of Airy beams: dependence upon spatial coherence and wavelength," Opt. Express **17**, 13236–13245 (2009).

PUBLICATIONS

CURRICULUM VITAE

Name: Peeter Piksarv
Date of birth: October 17, 1984
Citizenship: Estonian
Telephone: +372 5666 6623
Email: peeter.piksarv@eesti.ee

Education:

2009–…	University of Tartu, Doctorate studies, Physics
2007–2009	University of Tartu, Master's studies, Fundamental Physics
2003–2007	University of Tartu, Bachelor's studies, Physics

Professional employment:

2013–…	University of Tartu, Institute of Physics, Junior Research Fellow of Wave Optics
2009–2012	University of Tartu, Institute of Physics, Engineer

Professional self-improvement:

Aug 2010	66th Scottish Universities Summer School in Physics: International Summer School in Ultrafast Nonlinear Optics, Herriot–Watt University, Edinburgh, Scotland
Feb 2009	Practice at ultrafast optics research lab led by Prof. Rick Trebino, Georgia Institute of Technology, Atlanta, USA
Apr 2008	International Summer School for Training in Experimental Activity in the Field of Laser and Laser Applications, Foundation for Research and Technology, Heraklion, Greece

Honours and awards:

2009	Student Research Prize of the Estonian Academy of Sciences, 1st award (for master thesis)
2009	Student Research Prize of the Estonian Ministry of Education and Research, Honorary mention (for master thesis)

ELULOOKIRJELDUS

Nimi: Peeter Piksarv
Sünniaeg: 17. oktoober 1984
Kodakondsus: Eesti
Telefon: 5666 6623
E-post: peeter.piksarv@eesti.ee

Haridustee:

2009–…	Tartu Ülikool, doktoriõpe, füüsika
2007–2009	Tartu Ülikool, magistriõpe, fundamentaalfüüsika
2003–2007	Tartu Ülikool, bakalaureuseõpe, füüsika

Erialane teenistuskäik:

2013–…	Tartu Ülikooli Füüsika Instituut, laineoptika nooremteadur
2009–2012	Tartu Ülikooli Füüsika Instituut, insener

Erialane enesetäiendus:

aug 2010	"66th Scottish Universities Summer School in Physics: International Summer School in Ultrafast Nonlinear Optics 2010" suvekool, Herriot–Watt University, Edinburgh, Šotimaa
veebr 2009	Praktika prof Rick Trebino juhitavas ülikiire optka laboris, Georgia Institute of Technology, Atlanta, USA
apr 2008	"International Summer School for Training in Experimental Activity in the field of Laser and Laser Application" suvekool, Foundation for Research and Technology, Iraklion, Kreeka.

Erialane tunnustus:

2009	Eesti Teaduste Akadeemia üliõpilaste teadustööde konkursi I preemia (magistritöö eest)
2009	Haridus- ja Teadusministeeriumi üliõpilaste teadustööde riikliku konkursi diplom (magistritöö eest)

DISSERTATIONES PHYSICAE UNIVERSITATIS TARTUENSIS

1. **Andrus Ausmees.** XUV-induced electron emission and electron-phonon interaction in alkali halides. Tartu, 1991.
2. **Heiki Sõnajalg.** Shaping and recalling of light pulses by optical elements based on spectral hole burning. Tartu, 1991.
3. **Sergei Savihhin.** Ultrafast dynamics of F-centers and bound excitons from picosecond spectroscopy data. Tartu, 1991.
4. **Ergo Nõmmiste.** Leelishalogeniidide röntgenelektronemissioon kiiritamisel footonitega energiaga 70–140 eV. Tartu, 1991.
5. **Margus Rätsep.** Spectral gratings and their relaxation in some low-temperature impurity-doped glasses and chrystals. Tartu, 1991.
6. **Tõnu Pullerits.** Primary energy transfer in photosynthesis. Model calculations. Tartu, 1991.
7. **Olev Saks.** Attoampri diapasoonis voolude mõõtmise füüsikalised alused. Tartu, 1991.
8. **Andres Virro.** AlGaAsSb/GaSb heterostructure injection lasers. Tartu, 1991.
9. **Hans Korge.** Investigation of negative point discharge in pure nitrogen at atmospheric pressure. Tartu, 1992.
10. **Jüri Maksimov.** Nonlinear generation of laser VUV radiation for high-resolution spectroscopy. Tartu, 1992.
11. **Mark Aizengendler.** Photostimulated transformation of aggregate defects and spectral hole burning in a neutron-irradiated sapphire. Tartu, 1992.
12. **Hele Siimon.** Atomic layer molecular beam epitaxy of A^2B^6 compounds described on the basis of kinetic equations model. Tartu, 1992.
13. **Tõnu Reinot.** The kinetics of polariton luminescence, energy transfer and relaxation in anthracene. Tartu, 1992.
14. **Toomas Rõõm.** Paramagnetic H^{2-} and F^+ centers in CaO crystals: spectra, relaxation and recombination luminescence. Tallinn, 1993.
15. **Erko Jalviste.** Laser spectroscopy of some jet-cooled organic molecules. Tartu, 1993.
16. **Alvo Aabloo.** Studies of crystalline celluloses using potential energy calculations. Tartu, 1994.
17. **Peeter Paris.** Initiation of corona pulses. Tartu, 1994.
18. **Павел Рубин.** Локальные дефектные состояния в CuO_2 плоскостях высокотемпературных сверхпроводников. Тарту, 1994.
19. **Olavi Ollikainen.** Applications of persistent spectral hole burning in ultrafast optical neural networks, time-resolved spectroscopy and holographic interferometry. Tartu, 1996.
20. **Ülo Mets.** Methodological aspects of fluorescence correlation spectroscopy. Tartu, 1996.
21. **Mikhail Danilkin.** Interaction of intrinsic and impurity defects in CaS:Eu luminophors. Tartu, 1997.

39

22. **Ирина Кудрявцева.** Создание и стабилизация дефектов в кристаллах KBr, KCl, RbCl при облучении ВУФ-радиацией. Тарту, 1997.
23. **Andres Osvet.** Photochromic properties of radiation-induced defects in diamond. Tartu, 1998.
24. **Jüri Örd.** Classical and quantum aspects of geodesic multiplication. Tartu, 1998.
25. **Priit Sarv.** High resolution solid-state NMR studies of zeolites. Tartu, 1998.
26. **Сергей Долгов.** Электронные возбуждения и дефектообразование в некоторых оксидах металлов. Тарту, 1998.
27. **Kaupo Kukli.** Atomic layer deposition of artificially structured dielectric materials. Tartu, 1999.
28. **Ivo Heinmaa.** Nuclear resonance studies of local structure in $RBa_2Cu_3O_{6+x}$ compounds. Tartu, 1999.
29. **Aleksander Shelkan.** Hole states in CuO_2 planes of high temperature superconducting materials. Tartu, 1999.
30. **Dmitri Nevedrov.** Nonlinear effects in quantum lattices. Tartu, 1999.
31. **Rein Ruus.** Collapse of 3d (4f) orbitals in 2p (3d) excited configurations and its effect on the x-ray and electron spectra. Tartu, 1999.
32. **Valter Zazubovich.** Local relaxation in incommensurate and glassy solids studied by Spectral Hole Burning. Tartu, 1999.
33. **Indrek Reimand.** Picosecond dynamics of optical excitations in GaAs and other excitonic systems. Tartu, 2000.
34. **Vladimir Babin.** Spectroscopy of exciton states in some halide macro- and nanocrystals. Tartu, 2001.
35. **Toomas Plank.** Positive corona at combined DC and AC voltage. Tartu, 2001.
36. **Kristjan Leiger.** Pressure-induced effects in inhomogeneous spectra of doped solids. Tartu, 2002.
37. **Helle Kaasik.** Nonperturbative theory of multiphonon vibrational relaxation and nonradiative transitions. Tartu, 2002.
38. **Tõnu Laas.** Propagation of waves in curved spacetimes. Tartu, 2002.
39. **Rünno Lõhmus.** Application of novel hybrid methods in SPM studies of nanostructural materials. Tartu, 2002.
40. **Kaido Reivelt.** Optical implementation of propagation-invariant pulsed free-space wave fields. Tartu, 2003.
41. **Heiki Kasemägi.** The effect of nanoparticle additives on lithium-ion mobility in a polymer electrolyte. Tartu, 2003.
42. **Villu Repän.** Low current mode of negative corona. Tartu, 2004.
43. **Алексей Котлов.** Оксианионные диэлектрические кристаллы: зонная структура и электронные возбуждения. Tartu, 2004.
44. **Jaak Talts.** Continuous non-invasive blood pressure measurement: comparative and methodological studies of the differential servo-oscillometric method. Tartu, 2004.
45. **Margus Saal.** Studies of pre-big bang and braneworld cosmology. Tartu, 2004.

46. **Eduard Gerškevitš.** Dose to bone marrow and leukaemia risk in external beam radiotherapy of prostate cancer. Tartu, 2005.
47. **Sergey Shchemelyov.** Sum-frequency generation and multiphoton ionization in xenon under excitation by conical laser beams. Tartu, 2006.
48. **Valter Kiisk.** Optical investigation of metal-oxide thin films. Tartu, 2006.
49. **Jaan Aarik.** Atomic layer deposition of titanium, zirconium and hafnium dioxides: growth mechanisms and properties of thin films. Tartu, 2007.
50. **Astrid Rekker.** Colored-noise-controlled anomalous transport and phase transitions in complex systems. Tartu, 2007.
51. **Andres Punning.** Electromechanical characterization of ionic polymer-metal composite sensing actuators. Tartu, 2007.
52. **Indrek Jõgi.** Conduction mechanisms in thin atomic layer deposited films containing TiO_2. Tartu, 2007.
53. **Aleksei Krasnikov.** Luminescence and defects creation processes in lead tungstate crystals. Tartu, 2007.
54. **Küllike Rägo.** Superconducting properties of MgB_2 in a scenario with intra- and interband pairing channels. Tartu, 2008.
55. **Els Heinsalu.** Normal and anomalously slow diffusion under external fields. Tartu, 2008.
56. **Kuno Kooser.** Soft x-ray induced radiative and nonradiative core-hole decay processes in thin films and solids. Tartu, 2008.
57. **Vadim Boltrushko.** Theory of vibronic transitions with strong nonlinear vibronic interaction in solids. Tartu, 2008.
58. **Andi Hektor.** Neutrino Physics beyond the Standard Model. Tartu, 2008.
59. **Raavo Josepson.** Photoinduced field-assisted electron emission into gases. Tartu, 2008.
60. **Martti Pärs.** Study of spontaneous and photoinduced processes in molecular solids using high-resolution optical spectroscopy. Tartu, 2008.
61. **Kristjan Kannike.** Implications of neutrino masses. Tartu, 2008.
62. **Vigen Issahhanjan.** Hole and interstitial centres in radiation-resistant MgO single crystals. Tartu, 2008.
63. **Veera Krasnenko.** Computational modeling of fluorescent proteins. Tartu, 2008.
64. **Mait Müntel.** Detection of doubly charged higgs boson in the CMS detector. Tartu, 2008.
65. **Kalle Kepler.** Optimisation of patient doses and image quality in diagnostic radiology. Tartu, 2009.
66. **Jüri Raud.** Study of negative glow and positive column regions of capillary HF discharge. Tartu, 2009.
67. **Sven Lange.** Spectroscopic and phase-stabilisation properties of pure and rare-earth ions activated ZrO_2 and HfO_2. Tartu, 2010.
68. **Aarne Kasikov.** Optical characterization of inhomogeneous thin films. Tartu, 2010.

69. **Heli Valtna-Lukner.** Superluminally propagating localized optical pulses. Tartu, 2010.
70. **Artjom Vargunin.** Stochastic and deterministic features of ordering in the systems with a phase transition. Tartu, 2010.
71. **Hannes Liivat.** Probing new physics in e+e− annihilations into heavy particles via spin orientation effects. Tartu, 2010.
72. **Tanel Mullari.** On the second order relativistic deviation equation and its applications. Tartu, 2010.
73. **Aleksandr Lissovski.** Pulsed high-pressure discharge in argon: spectroscopic diagnostics, modeling and development. Tartu, 2010.
74. **Aile Tamm.** Atomic layer deposition of high-permittivity insulators from cyclopentadienyl-based precursors. Tartu, 2010.
75. **Janek Uin.** Electrical separation for generating standard aerosols in a wide particle size range. Tartu, 2011.
76. **Svetlana Ganina.** Hajusandmetega ülesanded kui üks võimalus füüsikaõppe efektiivsuse tõstmiseks. Tartu, 2011
77. **Joel Kuusk.** Measurement of top-of-canopy spectral reflectance of forests for developing vegetation radiative transfer models. Tartu, 2011.
78. **Raul Rammula**. Atomic layer deposition of HfO_2 – nucleation, growth and structure development of thin films. Tartu, 2011.
79. **Сергей Наконечный.** Исследование электронно-дырочных и интерстициал-вакансионных процессов в монокристаллах MgO и LiF методами термоактивационной спектроскопии. Тарту, 2011.
80. **Niina Voropajeva.** Elementary excitations near the boundary of a strongly correlated crystal. Tartu, 2011.
81. **Martin Timusk.** Development and characterization of hybrid electro-optical materials. Tartu, 2012, 106 p.
82. **Merle Lust.** Assessment of dose components to Estonian population. Tartu, 2012, 84 p.
83. **Karl Kruusamäe.** Deformation-dependent electrode impedance of ionic electromechanically active polymers. Tartu, 2012, 128 p.
84. **Liis Rebane.** Measurement of the $W \to \tau\nu$ cross section and a search for a doubly charged Higgs boson decaying to τ-leptons with the CMS detector. Tartu, 2012, 156 p.
85. **Jevgeni Šablonin.** Processes of structural defect creation in pure and doped MgO and NaCl single crystals under condition of low or super high density of electronic excitations. Tartu, 2013, 145 p.
86. **Riho Vendt**. Combined method for establishment and dissemination of the international temperature scale. Tartu, 2013, 108 p.